A Volcano Rekindled: The Renewed Eruption of Mount St. Helens, 2004–2006
Edited by David R. Sherrod, William E. Scott, and Peter H. Stauffer
U.S. Geological Survey Professional Paper 1750, 2008

Chapter 4

Absolute and Relative Locations of Earthquakes at Mount St. Helens, Washington, Using Continuous Data: Implications for Magmatic Processes

By Weston A. Thelen[1], Robert S. Crosson[2], and Kenneth C. Creager[2]

Abstract

This study uses a combination of absolute and relative locations from earthquake multiplets to investigate the seismicity associated with the eruptive sequence at Mount St. Helens between September 23, 2004, and November 20, 2004. Multiplets, a prominent feature of seismicity during this time period, occurred as volcano-tectonic, hybrid, and low-frequency earthquakes spanning a large range of magnitudes and lifespans. Absolute locations were improved through the use of a new one-dimensional velocity model with excellent shallow constraints on P-wave velocities. We used jackknife tests to minimize possible biases in absolute and relative locations resulting from station outages and changing station configurations. In this paper, we show that earthquake hypocenters shallowed before the October 1 explosion along a north-dipping structure under the 1980–86 dome. Relative relocations of multiplets during the initial seismic unrest and ensuing eruption showed rather small source volumes before the October 1 explosion and larger tabular source volumes after October 5. All multiplets possess absolute locations very close to each other. However, the highly dissimilar waveforms displayed by each of the multiplets analyzed suggest that different sources and mechanisms were present within a very small source volume. We suggest that multiplets were related to pressurization of the conduit system that produced a stationary source that was highly stable over long time periods. On the basis of their response to explosions occurring in October 2004, earthquakes not associated with multiplets also appeared to be pressure dependent. The pressure source for these earthquakes appeared, however, to be different from the pressure source of the multiplets.

Introduction

Because more than 1 million earthquakes occurred between the beginning of the latest eruption of Mount St. Helens in 2004 and the end of 2005 (Moran and others, this volume, chap. 2), there is a need to locate a representative set of earthquakes to search for first-order patterns and trends that may aid in future monitoring and research. Although locating most of the 1 million earthquakes would be possible and even somewhat practical with current methods and parallel computing, such a study is beyond the scope of this paper. Herein we concentrate on the seismicity leading up to the early October explosions and through about 1 month of dacitic dome building in order to characterize the seismicity associated with each eruptive phase.

One of the most striking features in this eruption's seismicity was the prominence of earthquake multiplets, or repetitious earthquakes. Earthquake multiplets are characteristically defined by their highly similar waveforms, often exceeding cross-correlation coefficients of 0.8 (Geller and Mueller, 1980; Frémont and Malone, 1987; fig. 1). This phenomenon is likely caused by earthquakes occurring very close to the same location with a similar source process (Geller and Mueller, 1980). Earthquake multiplets are a common occurrence in tectonic and volcanic areas worldwide, and many authors have exploited earthquake multiplets to determine highly precise relative relocations (for example, Poupinet and others, 1984; Fréchet, 1985; Frémont and Malone, 1987; Got and others, 1994; Waldhauser and Ellsworth, 2000). Every relative relocation method operates on the basic idea that closely spaced

[1] Pacific Northwest Seismic Network, Department of Earth and Space Sciences, University of Washington, Box 351310, Seattle, WA 98195

[2] Department of Earth and Space Sciences, University of Washington, Box 351310, Seattle, WA 98195

earthquakes recorded at a common station will have similar path and site effects. As long as the source region is homogeneous (or reasonably so) with respect to the dominant wavelength of the waveforms, the relative time lag between the earthquakes is a measure of the separation distance between the sources (Wolfe, 2002).

The classification and description of large suites of multiplets is also fairly common on volcanoes worldwide. Got and others (1994) relocated 250 earthquakes beneath Kīlauea, Hawai‘i, to define a nearly horizontal plane of seismicity at 8-km depth. Stevens and Chouet (2001) analyzed long-period multiplets beneath Redoubt Volcano before its 1989 eruption and found smooth changes in amplitude and cross-correlation coefficient within multiplets. Rowe and others (2004) relocated approximately 17,000 similar earthquakes on Soufrière Hills volcano, Montserrat, by identifying multiplets through a hierarchical clustering algorithm and using those multiplets as stacks to refine phase picks. On Mount Pinatubo, Philippines, Battaglia and others (2004) used a similar approach to that of Got and others (1994) to relocate almost 11,000 events.

When locating similar earthquakes, a common approach is to use manually phase-picked events to seed stacks of similar events. Short windows of data are normally used, usually between 1.28 and 2.56 s after the P-wave arrival. Often such studies use triggered waveform data (records started by an amplitude trigger at the seismometer) instead of continuous waveform data, which are used here to identify multiplets. Past data sets are thus limited by what is triggered or located manually by the local seismic network and may be largely incomplete (Rowe and others, 2004).

Beginning in 1980, Mount St. Helens has been the most seismically active volcano in the Cascade Range. Increases in moment release in the shallow edifice are characteristically associated with explosive and effusive eruptions (Swanson and others, 1983). Earthquake multiplets at shallow depths were commonly observed at Mount St. Helens after 1982 and were used to obtain highly precise relative locations of earthquakes during the dome-building eruptions of September 10, 1984, and May–June 1985 (Frémont and Malone, 1987). Musumeci and others (2002) used similar events during the late 1990s to establish continuing magma recharge after 1992 into a storage zone at 5.5–10-km depth.

Since the beginning of the latest eruption in September 2004, less than 1 percent of the earthquakes detected have been routinely processed by the Pacific Northwest Seismic Network (PNSN) (Qamar and others, this volume, chap. 3), although care has been taken by PNSN analysts to extract a representative sampling of waveforms for the PNSN earthquake catalog. In this paper we (1) relocate the triggered earthquakes from the PNSN catalog to establish absolute locations, (2) identify and locate multiplets from the continuous seismic record, and (3) discuss the volcanological significance of our findings. We do not claim to classify every earthquake that has occurred during this period; instead, we present the absolute locations of the PNSN catalog data with a new velocity model and the characteristics of a representative set of multiplets that exhibit large populations and/or long lifespans. Especially of interest in this study are the relative locations and characters of the individual multiplets, how those characteristics change through time, and the relation of those characteristics to other phenomena. This information is important because we would like to assess the ability of multiplets to forecast eruptive activity or style.

This paper follows the time divisions used by Moran and others (this volume, chap. 2) to present the seismic evolution of the eruption. As it happens, station outages or station installations necessitated the use of additional time breaks to present consistent locations within a time period. Care has been taken across changes in network configurations to present a consistent and coherent picture of the seismicity.

Methods

Absolute Locations

Mount St. Helens has the densest seismic network of any volcano in the Pacific Northwest. Before the eruption in 2004, there were 13 permanent stations within 20 km of the volcano (fig. 2). Except for 11 days after the first phreatic explosion on October 1, a seismometer was positioned within 1 km of the new vent (McChesney and others, this volume, chap. 7), an arrangement that allowed an unusually accurate determination of absolute locations beneath the edifice compared to standard regional network locations. In this paper, we consider only earthquakes with eight picked P-wave arrival times, a maximum azimuthal gap of 135 degrees, and an arrival time pick within 3 km of the epicenter. The 3-km criterion is necessary for times when stations on the 1980s dome were saturated or destroyed. Additionally, we use a new velocity model (Thelen and others, 2006) to significantly reduce station corrections and improve locations (table 1, appendix 1). Absolute locations are determined with the program “SPONG,” a PNSN adaptation of FASTHYPO (Herrmann, 1979).

Uncertainties in absolute event location are given by the program SPONG, which was benchmarked against Hypoinverse (Klein, 1989; S. Malone, oral commun., 2006). These include uncertainties in phase picks and in the earthquake-location inversion scheme itself. To evaluate the effect of changing station configurations, we performed jackknife tests (Efron and Gong, 1983) by systematically removing seismic stations. Generally, removing crater stations reduced depth constraint but did not change the distribution of epicenters significantly (appendix 2). The reduced resolution in depth often produced “airquakes,” earthquakes with phase picks that resulted in depths above the velocity-model datum used in the solution. Airquakes were common in the existing PNSN earthquake catalog throughout the eruptive sequence at Mount St. Helens beginning in 2004. The uncertainties presented here do not include uncertainties in the velocity model, do not quantitatively account for changes in station configuration, and therefore are likely underestimates, especially in depth.

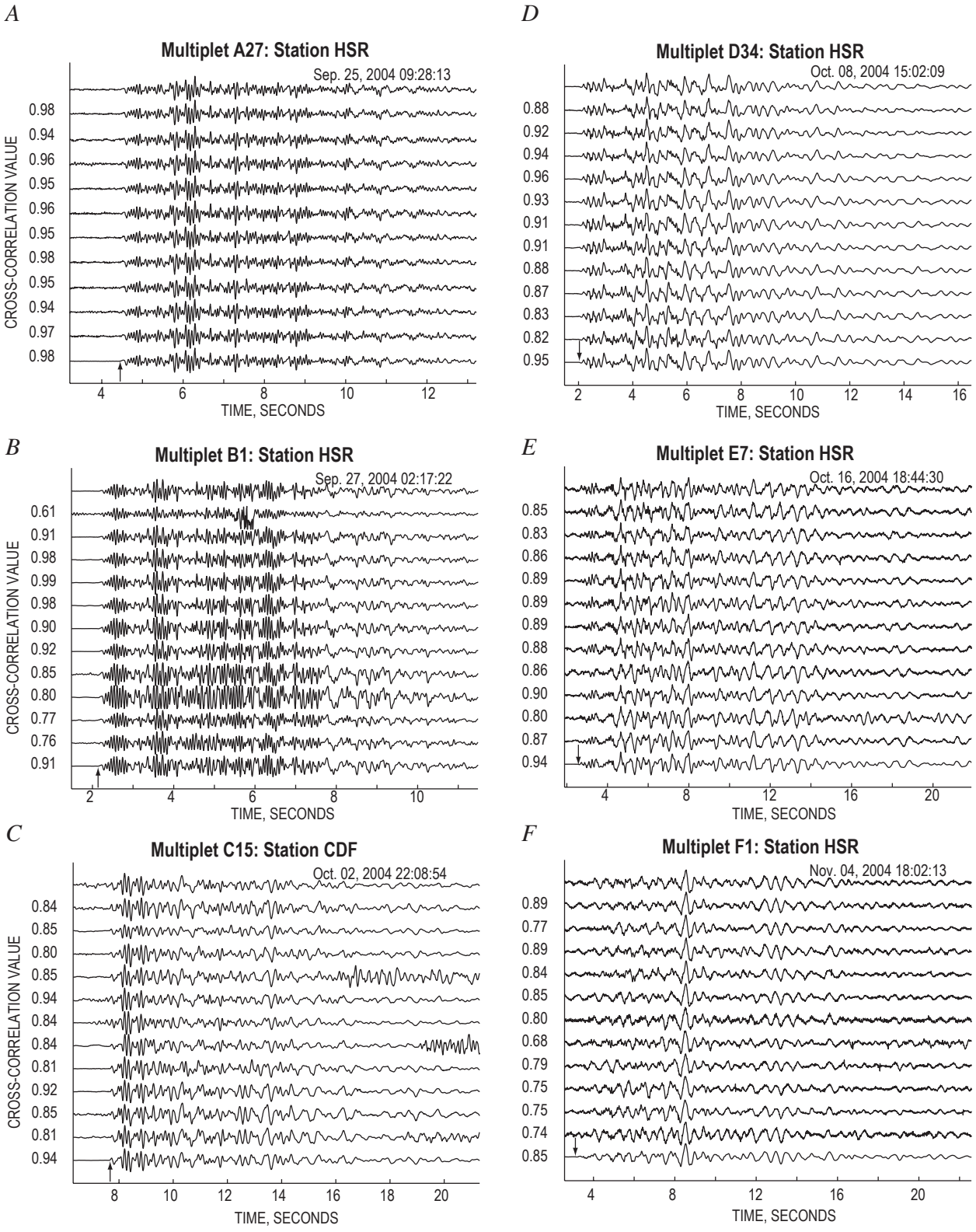

Figure 1. Example of waveforms from six multiplets analyzed in this study. Top trace in each is seed event for multiplet, and last trace is stack of all waveforms within multiplet at given station. Date and time on first trace are when seed event occurred. Arrow in bottom trace shows first arrival with polarity (up is compressional, down is dilatational). Station CDF has reversed polarity, so the first motion in *C* is actually down. Cross-correlation value of each trace with respect to seed event is shown on the y-axis. Waveforms are unfiltered and chosen at constant time intervals within the lifespan of their respective multiplets.

Classification of Multiplets

The PNSN catalog contains less than 1 percent of the total number of earthquakes, so entire groups of earthquakes have no representative in the catalog. As a result, we could not use the PNSN catalog as a starting point in searching for multiplets. Instead, our method for identifying multiplets started with a simple, highly sensitive threshold autopicker for which we selected a window of data around each trigger on the basis of the characteristic length of earthquakes in a given time period (10–20 s). Our autopicker typically missed the P-wave first arrival, so we included an empirically determined amount of time before the trigger (usually 1–3 s) in order to capture the entire event.

After the triggers were selected from the record, we cross-correlated, in the time domain, the first event to all other events at a particular station. Any event that was equal to or above the threshold cross-correlation coefficient (0.8) was considered part of that multiplet. The multiplet was then taken from the triggered events and stored. The next event that was not part of an existing multiplet was cross-correlated against all the remaining events and evaluated for events exceeding the cross-correlation coefficient cutoff. Any event that did not correlate with another event was considered an orphan and stored else-

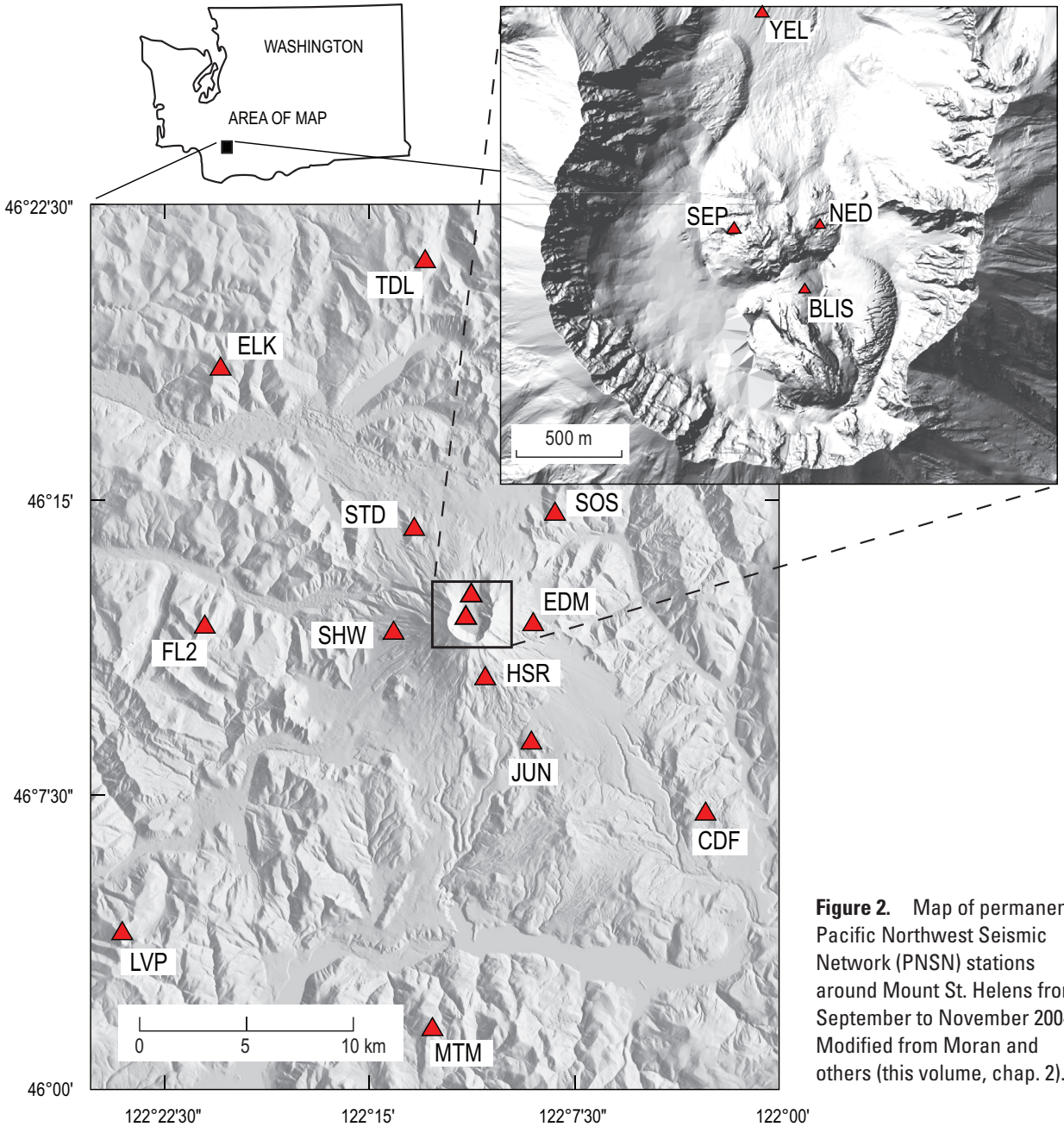

Figure 2. Map of permanent Pacific Northwest Seismic Network (PNSN) stations around Mount St. Helens from September to November 2004. Modified from Moran and others (this volume, chap. 2).

Table 1. Depth and velocity for P-wave model of Thelen and others (2006).

[Depth to top of layers defined by P-wave velocities; datum is altitude 2,200 m above sea level. Column 3 is the velocity model used for the relative locations, which assumes a Poisson solid in order to convert to S-wave velocity from the P-wave velocity of the one-dimensional model (appendix 1).]

Depth (km)	P-wave velocity (km/s)	S-wave velocity (km/s)
0	2.7	1.51
1.0	3.5	1.97
1.3	4.3	2.42
1.6	5.1	2.87
3.9	6.0	3.37
6.5	6.2	3.58
10.5	6.6	3.82
18.5	6.8	3.93
34.5	7.1	4.10
43.5	7.8	4.51

where. This process was repeated until all events were either classified into a multiplet or as an orphan. The multiplets were visually inspected to remove those with systematic noise such as calibration pulses and telemetry spikes, which can produce repeatable waveforms. Computer memory restrictions and the large number of triggers allowed us to process only about 10 days of data at a time. We therefore treated each time period individually and then combined the time periods by stacking multiplets from each time period and running the same analysis described above with event stacks instead of triggered data. This method served to combine time periods; however it also allowed for events with similar stacks to be combined even if individual events did not correlate at the initial threshold level. This technique of tracking multiplets has a disadvantage of using only one station to identify and classify multiplets, which makes it susceptible to near-site effects. However, Stephens and Chouet (2001) successfully used only one station to classify the multiplets before the 1989 eruption of Redoubt Volcano. We also visually checked other stations at the same distance range for the presence of the larger multiplets and ensured that near-site effects were not dominating the multiplet analysis.

Relative Location of Multiplets

After the identification of a multiplet, a representative event from that multiplet was chosen and cross-correlated against each hour of continuous data. Again, cross-correlation windows of 10–20 s were used, a choice based on the length of high signal-to-noise ratios throughout the waveform. Cross-correlation coefficients above a threshold were considered triggers. Three stations were required to have coincident triggers in order for the earthquake to be classified as a valid event. After the triggered events were compiled, all of the events were cross-correlated against each other at each station, and lags were noted at the maximum cross-correlation coefficient. Subsample estimates of lags were achieved in the time domain through polynomial interpolation of the cross-correlation coefficient peak. Lags were weighted by their normalized cross-correlation coefficient, and only lags with a cross-correlation above 0.8 were considered for earthquake locations. The lags for each event were then used to compute double-difference hypocenter locations with the hypoDD software (Waldhauser, 2001). For the initial location of the earthquakes within each multiplet, we stacked the multiplet and picked the first arrival of the stack at each station. Those picks were then applied to each earthquake in the stack on the basis of the lag derived from the cross-correlation. The picks were used to get absolute locations for each earthquake in the multiplet using the identical process as discussed above.

The use of long time windows meant that we were correlating dominantly S waves and Rayleigh waves. Most of the stations used in this study had a difference of 2 s or less between the P- and S-wave arrivals, meaning that at least 80 percent of the correlation window was composed of S waves and Rayleigh waves. Consequently, cross-correlating long time windows produced lags of phases that are traveling at S-wave velocities between the source and the receiver. We therefore elected to use an S-wave model for our relative locations. The S-wave model was obtained by assuming a Poisson's ratio for the crust and applying it to the P-wave model used in the absolute locations (table 1).

Errors in relative locations have several sources of uncertainty. One source is waveform alignment. Poorly aligned waveforms at a particular station may generate lineations in events toward that station (Battaglia and others, 2004). We minimized this source of uncertainty by using large time windows, which minimizes the occurrence of poorly aligned waveforms (Schaff and others, 2004). Another source of error in relative locations is uncertainty in the velocity model that the initial hypocenters start in (Michelini and Lomax, 2004). The path is canceled out by calculating the lag between two events, but the takeoff angle and azimuth are affected by the choice of an initial velocity model. In our analysis, we use a velocity model that is homogenous in the region of our cluster centroid. Changes in velocity, and therefore takeoff angle, only stretch or compress our cloud of hypocenters and do not affect the overall shape (appendix 3). Finally, artifacts in relative earthquake locations can be introduced through inhomogeneous phase lags on all stations in a solution. In other words, some stations will have a larger effect on the earthquake location than others, depending on the number of phase picks on that station. We tested this with the use of a jackknife test (Efron and Gong, 1983), a method in which one station is removed at a time and then all of the earthquakes within the multiplet are relocated, using the reduced station set (appendix 3). The change in location of each earthquake

was tracked, and the maximum offset of all of the stations in the north, east, and vertical directions is presented as the uncertainty in relative location.

September 23–October 5, 2004: Vent-Clearing Phase

Absolute Locations, September 23, 0000 PDT, Through September 25, 1200 PDT

Relocating a subset of catalog PNSN events with the updated velocity model revealed a tight cluster of earthquakes with a radius of 250 m centered immediately southeast of station SEP (fig. 3*A*). The depth cross section showed a cluster of hypocenters that was elongate toward the future vent. The cluster spanned depths of approximately 400 to 1,100 m below the future vent. The average number of phases used in the earthquake location during this time period was 9.32, with a maximum of 52. The mean azimuthal gap in this subset of earthquake locations was 90 degrees. A total of 229 earthquakes were relocated with formal uncertainties averaging 132, 92 and 84 m in the north, east, and vertical directions, respectively. Reductions in estimated uncertainties for the north, east, and vertical directions were 20, 35, and 74 percent when compared to the routine network locations.

Multiplets, September 23, 0000 PDT, Through September 25, 1200 PDT

The buildup of multiplets occurred at an accelerating pace until approximately 0200 on September 24 (fig. 4). All multiplets were composed of volcano-tectonic (VT) events and, in most cases, many multiplets were occurring simultaneously. Here we distinguish VT earthquakes from hybrid and low-frequency earthquakes, as was done by Moran and others (this volume, chap. 2). Examples of frequency spectra of hybrid versus low-frequency earthquakes versus VT earthquakes, as defined in this paper, are shown in figure 5. The maximum number of multiplets with populations greater than 20 occurring concurrently was eight at 0200 PDT on September 24, coincident with the maximum of earthquake amplitudes on station JUN during this time period (fig. 4). After the maximum in earthquake amplitudes on September 24, seismic activity waned until September 26. None of the early multiplets recurred after seismic activity ramped up again on September 26, 2004.

The largest magnitude multiplet during this period, A27 (figs. 1, 6), was a group of 59 VT events that occurred over approximately 3 hours beginning at 1104 PDT on September 25. Picking the first arrivals of the stacked traces of A27 on each station and locating the multiplet with standard absolute-location techniques resulted in a location at the south end of the cluster of epicenters in figure 3*A*, at depths near the top of the cluster. The absolute location of the stack used only six phase picks, giving the location of the hypocentroid the largest uncertainty of any multiplet analyzed. Double-difference relocations of this swarm reveal a tight cluster, spanning less than 10 m in depth and about 5 m horizontally (fig. 6*A*). Orthogonal cross sections show mostly vertical orientations, which are an artifact of different stations' picks being used for different events. Uncertainty estimates are on the order of 3 m horizontally and 20 m vertically. In figure 6, the generally small average errors are masked by a few larger errors as great as 40 m. The cross-correlation values of the first event to subsequent events in the multiplet are nearly constant. Considering the location errors and constant cross-correlation values, we suggest that the earthquakes in this multiplet occurred at nearly the same location. The end of this multiplet coincided with the waning seismic activity of the swarm on September 25 (Moran and others, chap. 2, their figs. 4, 5).

Absolute Locations, September 25, 1200 PDT, Through October 1, 1200 PDT

Absolute locations of 313 PNSN catalog events during this time period showed a distinct shift up and to the south compared to those of the previous period (figs. 3*B*, 7). The decrease in earthquake depth was consistent with phase-pick differences identified by Moran and others (this volume, chap. 2; fig. 7) between September 25 and September 27. This cluster, too, was tightly spaced in depth (250 m radius) and in epicenter (300 m radius), with respect to other absolute locations. The hypocentroid shift compared to the swarm beginning September 23 was 133 m south, 69 m east, and 221 m up. The average number of stations used was 11, the average gap was 78 degrees, and the average distance from the epicenter to the closest station was 115 m. Uncertainties in event locations averaged 109 m north-south, 140 m east-west, and 119 m in depth.

Multiplets, September 25, 1200 PDT, Through October 1, 1659 PDT

Multiplets were present throughout this time period and occurred in two phases before the explosion on October 1 (fig. 4). The multiplets had lifespans of 1–2.5 days. Their first buildup started at approximately 1200 PDT on September 25, 2004. Accompanying an increase in the number and lifespan of the multiplets was an increase in the maximum amplitudes of the continuous data averaged over 1-minute intervals at station JUN (fig. 4). The second buildup started around midday on September 29 and continued until the explosion on October 1. The second phase is identified by the end of multiplets from the first phase of buildup and the occurrence of new multiplets. The transition coincided with a 250 percent increase in the maximum amplitude of signals recorded at station JUN (fig. 4). Thirteen multiplets that

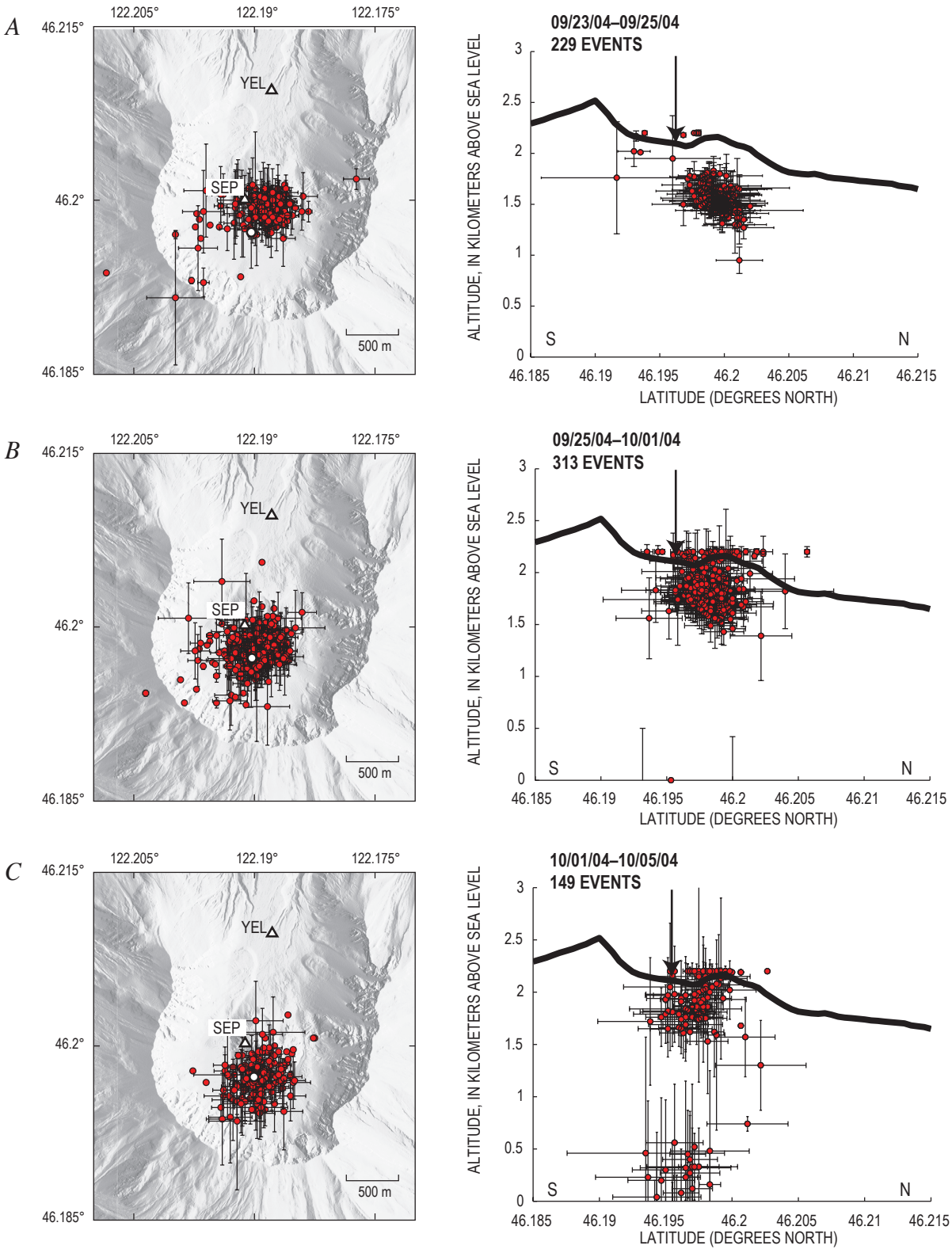

Figure 3. Absolute locations for Pacific Northwest Seismic Network (PNSN) catalog events for three time periods. Earthquakes plotted have eight or more phase picks, azimuthal gap of less than 135 degrees, and a phase pick at a station closer than 3 km from epicenter. Error bars are from SPONG location output. Permanent seismic stations shown on maps by black and white triangles. Cross sections show earthquake depth plots and topographic surface profile north-south through station SEP. White dot in map view and arrow in cross section show approximate location of vent.

were active before the October 1 explosion recurred after the explosion. Multiplets occurring after September 25 at 1200 PDT and through November 2004 were overwhelmingly hybrid and low-frequency earthquakes.

One multiplet, B1, started September 27 and continued for approximately 2.5 days (fig. 6*B*). The absolute location of the stacked traces formed a hypocentroid at 520-m depth, with an epicentroid centered in the cluster in figure 3*B*. The absolute location solution used 12 stations and had impulsive arrivals at all stations, making it one of the most reliable locations of the multiplets studied. The polarity of first arrivals was mixed and was consistent with reverse faulting on a north-striking, vertical or steeply dipping (85º–90º) fault. Relative locations of hypocenters are concentrated inside a sphere less than 15 m in diameter (fig. 6*B*). Location errors derived from jackknife techniques reveal uncertainties in the north, east, and vertical directions of 1.9 m, 1.3 m, and 1.3 m, respectively. The cross-correlation coefficient of the first event relative to each subsequent event decays with time, indicating a systematic temporal change in either the path between the earthquake and the receiver or a very small shift in location (Gret and others, 2005).

Absolute Locations, October 1, 1700 PDT, Through October 5, 1659 PDT

The absolute locations of 149 PNSN catalog events between the October 1 explosion and the end of October 5 apparently varied more widely in depth than those of the two previous time periods (fig. 3). However, with the destruction of station SEP during the October 1 explosion, the depths were less well constrained than in previous earthquake sets. In addition, emergent P-wave arrivals and overlapping codas made picks at the remaining crater station (YEL) and flank stations (HSR, EDM, SHW, and STD) sparse and imprecise, further affecting the depths. The effect of this can be seen as a cluster of seismicity that was falsely centered at 400-m

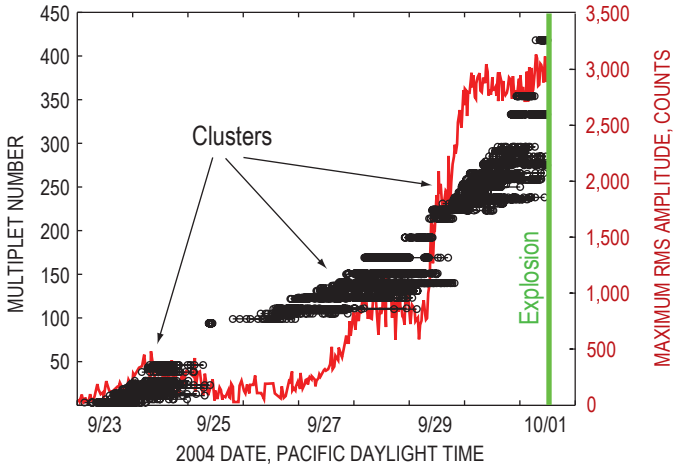

Figure 4. Timeline of multiplets from September 24, 2004, until explosion of October 1, 2004 (green line), detected on station HSR. Each earthquake is plotted as a circle, and multiplets are identified by a horizontal line through events that define multiplet. Only multiplets that have more than 20 events are plotted. Maximum root-mean-squared (RMS) amplitude averaged over 1 minute at station JUN shown in red.

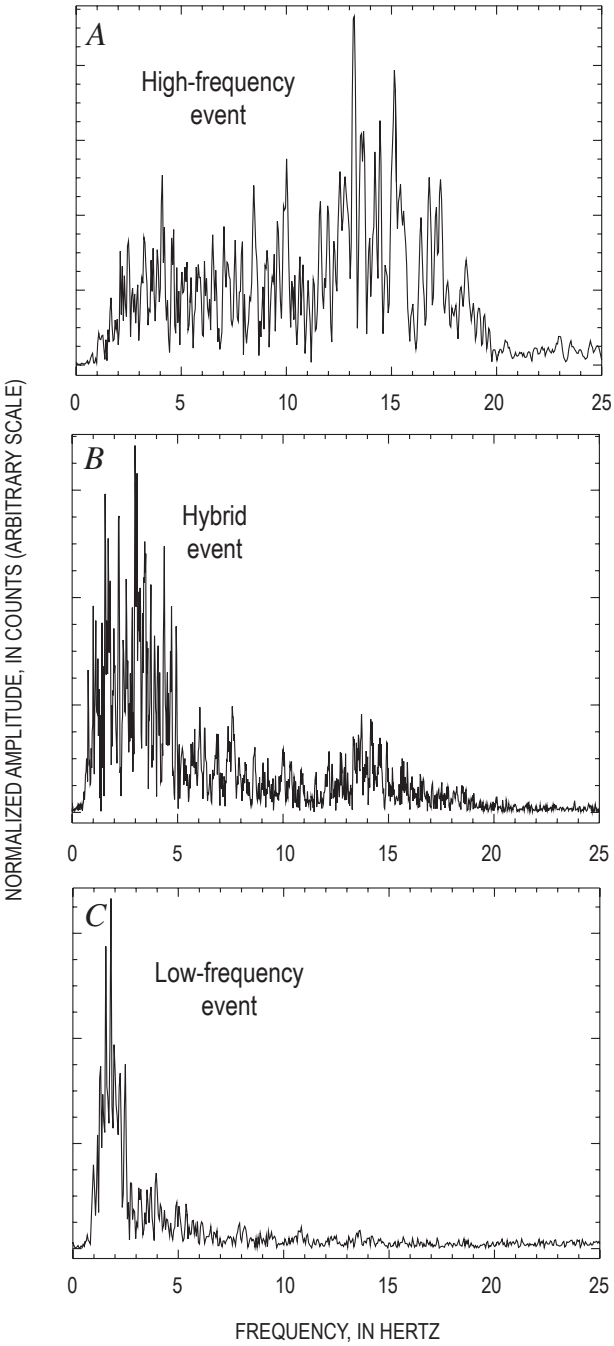

Figure 5. Examples of frequency spectra. High-frequency energy is seen between 12 and 20 Hz in high-frequency and hybrid events but not in low-frequency event. *A*, High-frequency event from September 25, 2004. *B*, Hybrid event from seed event of multiplet B1. *C*, Seed event of low-frequency multiplet F1 on station HSR.

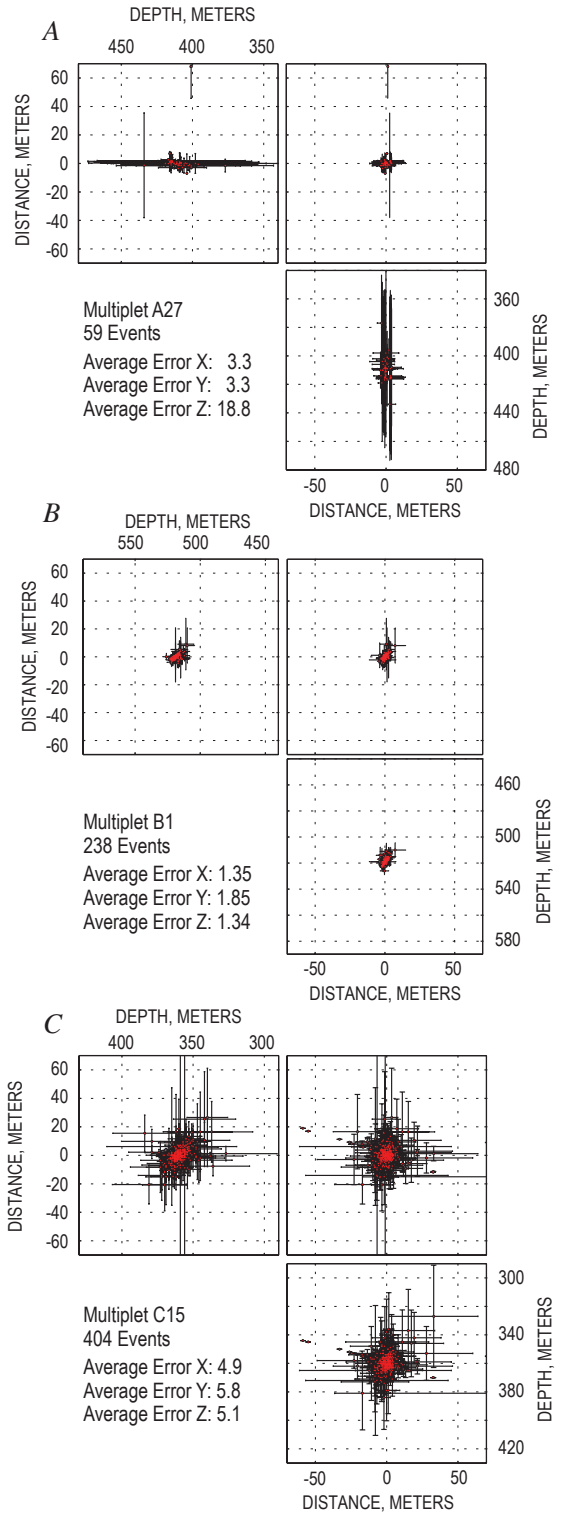

Figure 6. Relative relocations for three multiplets from the beginning of unrest through the period of phreatic explosions. For each, upper right square is map view (north at top), and left and bottom plots are cross sections. Plots are presented as cube with two sides folded out. Errors determined through jackknife techniques. Directions X, Y, and Z correspond to east, north, and vertical, respectively.

altitude owing to a lack of picks at station YEL (fig. 3*C*). Earthquake-location solutions used an average of 10 stations with an average gap of 81 degrees and an average delta of 1.52 km. Uncertainties in x, y, and z were 124, 146, and 244 m, respectively.

Multiplets, October 1, 1700 PDT, Through October 5, 1659 PDT

Several small-population multiplets were present during this time period (fig. 8). These multiplets consist of hybrid and low-frequency event families. There were three explosions and two episodes of tremor during this time period, in some cases concurrent with the start or stop of a multiplet. In most cases, however, multiplets during this time period continued largely unaffected by the occurrence of tremor or explosion.

One large low-frequency multiplet, C15, started 7 hours after the explosion on October 1. The absolute location of this multiplet using event stacks revealed a hypocentroid 100 m south and 160 m shallower than B1. Using a similar station configuration for both event stacks (no station SEP) shows approximately the same offset in location. Polarities from first arrivals of the multiplet stack were all dilatational, a characteristic for other earthquakes in this sequence, especially after October 1 (Moran and others, this volume, chap. 2; Qamar and others, this volume, chap. 3). This multiplet possessed highly stable amplitudes and cross-correlation coefficients in time. The relative relocations of 404 events from the C15 multiplet show a cluster of seismicity spanning approximately 20 m in diameter (fig. 6*C*). Some events of

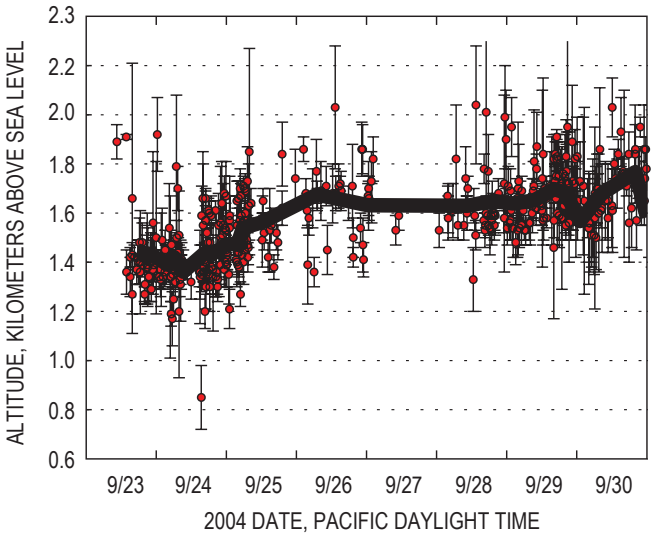

Figure 7. Earthquake altitude as function of time, September 23–30, 2004. Black line is running average altitude of 20 nearest earthquakes in time. The apparent gap in earthquakes between 9/26 and 9/28 is artificial, caused by a lack of earthquakes with location parameters that met our criteria and not by diminished seismicity.

the main cluster may have indicated a south-dipping structure; however, the overwhelming majority (75 percent) of the earthquake hypocenters were within the circular cluster. Using jackknife error techniques, we determined the locational uncertainties in north, east, and depth to be 5.8, 4.9, and 5.1 m, respectively.

October 5–November 20, 2004: Seismicity Associated with Dome Building

Absolute Locations, October 5, 0000 PDT, Through October 11, 1659 PDT

As with those between October 1 and October 5, earthquake arrivals at crater and flank stations were highly contaminated with earthquake codas from previous earthquakes and plagued with emergent signals. Thus, large uncertainties existed in the absolute locations, particularly in depth (fig. 9*A*). The spread of earthquake depth is suspect, owing to the absence of station SEP and the poor character of the first arrivals on station YEL. During this time period the absolute-location solutions of 227 events used an average of 10 stations, with an average gap of 89 degrees. The average distance to the nearest station was 1.15 km. Average uncertainties were 142 m in the north-south direction, 130 m in the east-west direction, and 226 m in depth.

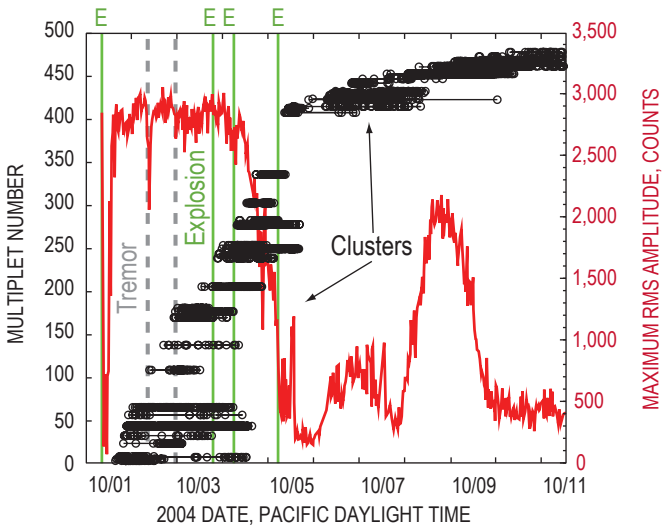

Figure 8. Timeline of multiplets from explosion of October 1 (leftmost green line) through October 11, 2004, detected on station ELK. Each earthquake is plotted as a circle, and multiplets are identified by a horizontal line through events that define multiplet. Only multiplets having more than 20 events are plotted. Maximum root-mean-squared (RMS) amplitude averaged over 1 minute at station JUN shown in red. Explosions, vertical green lines; tremor episodes, vertical gray lines.

Multiplets, October 5, 0000 PDT, Through October 11, 1659 PDT

Although four multiplets continued briefly through the explosion on October 5, a new temporal group of multiplets began about 1200 PDT on October 5. These multiplets generally had longer lifespans than previous multiplets, and fewer multiplets were occurring at the same time. Hybrids and low-frequency earthquakes dominated the seismic record. Multiplets during this time period did not obviously correspond to changes in the maximum amplitudes of signals recorded on station JUN.

The D34 hybrid multiplet discussed by Moran and others (this volume, chap. 2, their fig. 11) occurred during this time period. This multiplet consisted of 681 events starting October 8 at 0200 PDT. Absolute locations determined from the first arrivals of event stacks revealed a hypocentroid in the same location as multiplet C15. As was the case for C15, the polarities of the first arrivals were all dilatational. This multiplet methodically increased its amplitude before reaching a plateau and then decreased again to near the initial amplitude level (Moran and others, this volume, chap. 2). Magnitudes at the beginning were in the range M_d 1–1.5 and at the maximum were M_d 2.5–3.0. The cross-correlation coefficient of the first event to all others declined until the plateau in amplitude, and then remained constant for the rest of the sequence. Relative relocations of this cluster reveal a different pattern from that in previous multiplets. The hypocenter volume was tabular, striking to the southwest (fig. 10*A*). Uncertainties derived from jackknife tests showed errors of 2.7, 2.3, and 2.5 m, in the north-south, east-west, and vertical directions, respectively.

Absolute Locations, October 11, 1700 PDT, Through November 4, 1559 PST

During this period, low-frequency earthquakes dominated the seismic record. These earthquakes possessed emergent arrivals and thus had high uncertainties in absolute locations (fig. 9*B*). Earthquakes were extremely difficult to pick at stations outside the crater because of coda interference from previous events and poor arrivals. On October 12, station BLIS was installed on the saddle between the old and new domes (McChesney and others, this volume, chap. 7; fig. 2 for location). This station was used in less than half of the locations, however, owing to consistently emergent arrivals. Over the period of a month, only 130 earthquakes located by the PNSN met our selection criteria. For these earthquakes, an average of 10 stations were used for location solutions, with an average gap of 96 degrees and an average distance to the closest station of 431 m. Uncertainties in the north-south, east-west, and vertical directions were 142, 130, and 227 m, respectively.

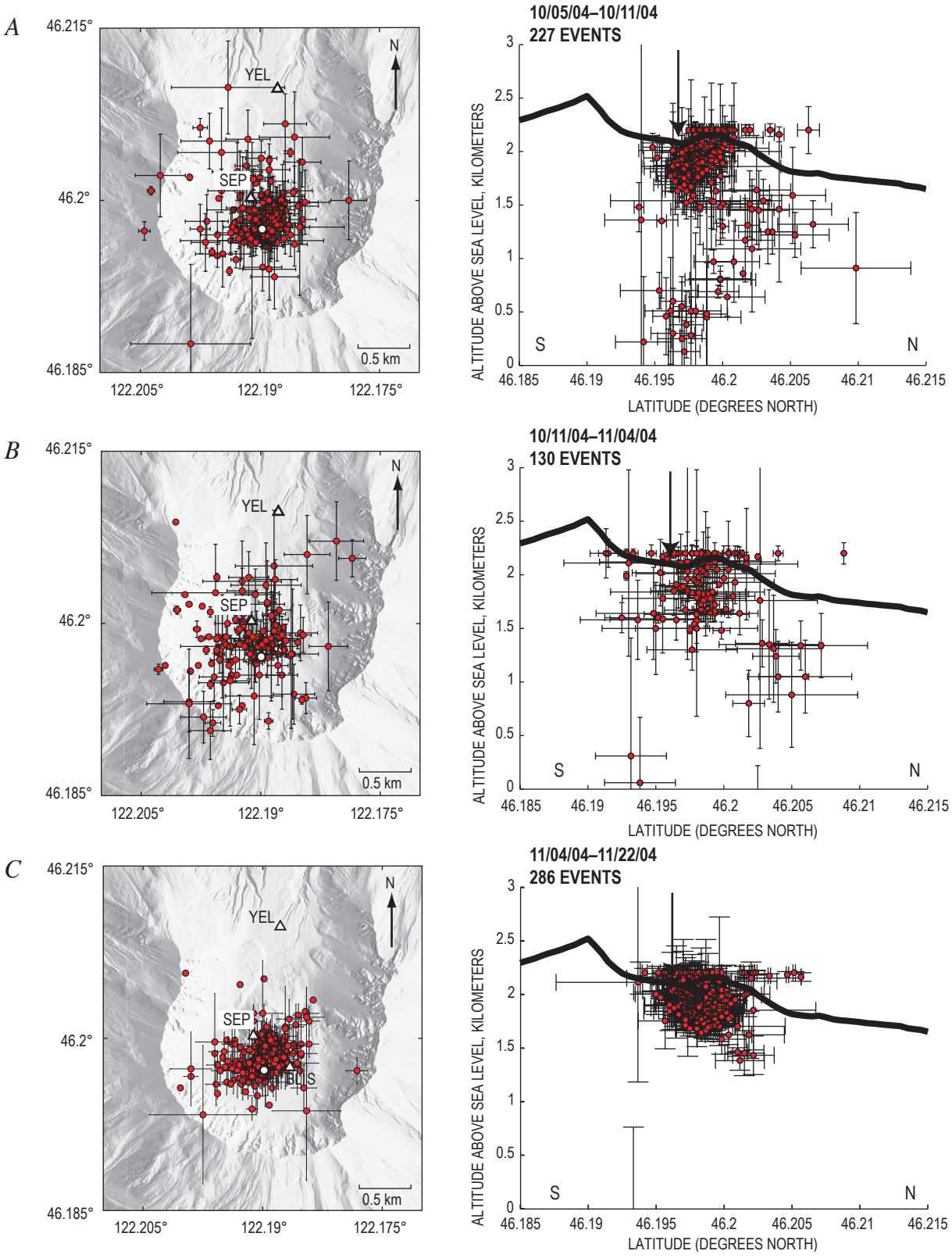

Figure 9. Absolute locations for Pacific Northwest Seismic Network (PNSN) catalog events for given time periods. Map views shown on left, cross sections on right. Permanent PNSN seismic stations shown with white triangles. Cross sections are north-south through station SEP, which was destroyed by explosion on October 1 and not reinstalled until November 5, 2004 (shown in top two plots only for reference). Earthquakes selected using same criteria as in figure 3. White dot (map view) and black arrow (cross section) show approximate location of vent.

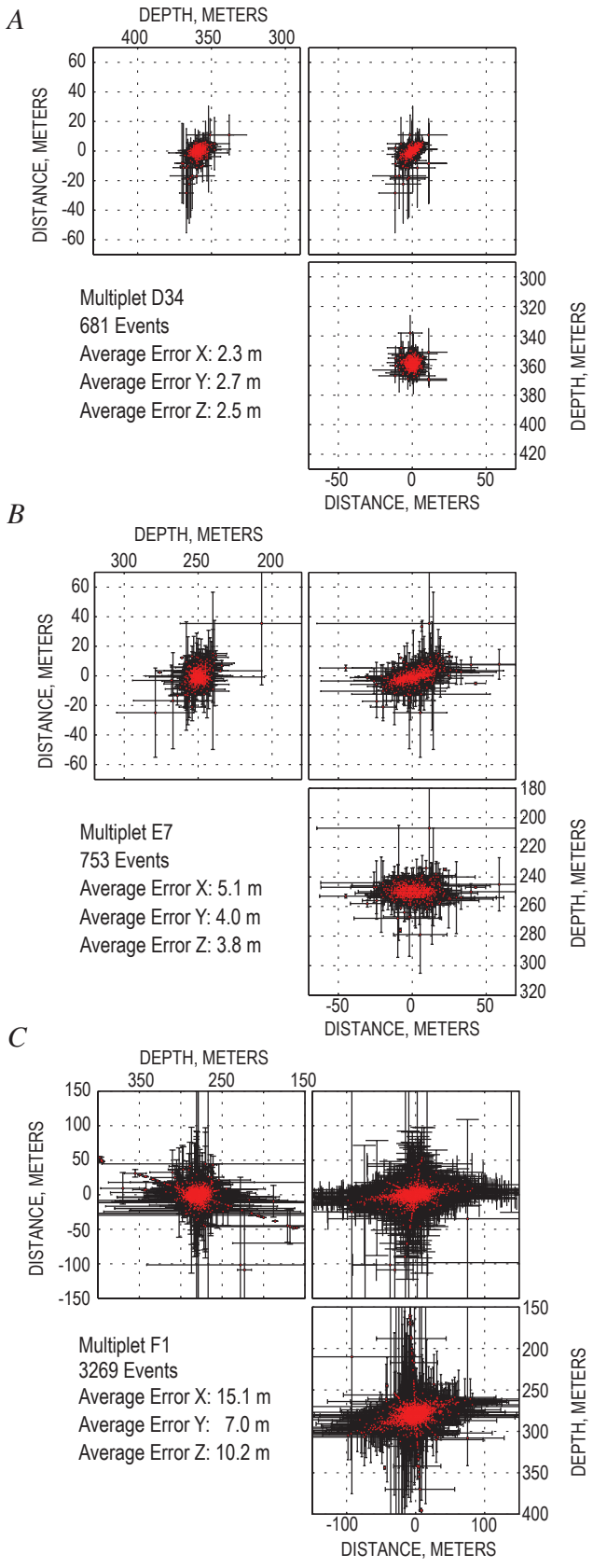

Figure 10. Relative relocations for three multiplets from early October to late November 2004. See figure 6 for explanation of views and errors.

Multiplets, October 11, 1700 PDT, Through November 4, 1559 PST

October 11, 2004, marked the first time new lava was seen at the surface (Vallance and others, this volume, chap. 9). Between then and November 4, three different spines were extruded, accompanied by comparatively low seismicity rates. Multiplets in the beginning of this time period had lifespans comparable to multiplets beginning after the October 5 explosion (figs. 8, 11), but multiplets with lifespans more than 1 month long began to occur later in the study period. In general, multiplets starting after October 22, 2004, had substantially longer lifespans than earlier multiplets. However, there was no obvious correlation between spine extrusion and the occurrence of multiplets during this time period.

One multiplet, E7, consisted of 753 events and started on October 16. Peak-to-peak amplitudes were stable and the cross-correlation coefficients of the first event compared to all others were nearly constant. The absolute hypocentroid from first-arrival picks of event stacks resulted in a location similar to that of multiplets C15 and D34. The polarities of first arrivals from event stacks all showed dilatation. The distribution of hypocenters was tabular, like that of D34, but had a more westerly strike (fig. 10*B*). The tabular distribution of epicenters had a long axis of approximately 40 m and a short axis of 10 m or less. The relative hypocenters spanned depths from 240 to 260 m. Uncertainties derived from jackknife analyses revealed average errors in location of 4.0, 5.1, and 3.8 m in the north-south, east-west, and vertical directions, respectively.

Absolute Locations, November 4, 1600 PST, Through November 22, 1559 PST

On November 5, station SEP was reinstalled (McChesney and others, this volume, chap. 7), increasing to three the number of stations within 2 km of the actively extruding spine. This addition proved important for locating earthquakes, as there were reliable picks from three close-in stations for almost all events. Absolute locations for 286 PNSN catalog events showed a 300-m-radius cluster with an epicentroid located only 160 m from the active vent (fig. 9*C*). The hypocentroid was located less than 400 m below the surface. The addition of the closest station, BLIS, on October 12, improved the sensitivity of the network to earthquakes, but comparing locations determined with and without BLIS is problematic. By ignoring station BLIS, we simulated the station configuration before October 1, 2004. The effect of taking out station BLIS was to make events slightly deeper on average, but the epicenters remained nearly unchanged. Details of these tests can be found in appendix 2. These tests suggest that the hypocentroid during this time period was at the same depth as the hypocentroid for the time period between September 25 and October 1, 2004, within error (figs. 3*B*, 6*C*). During the time period between November 4 and November 22, 2004, the earthquake-location solutions used an average of 10 stations, with an average gap of 96 degrees and

an average distance from the epicenter to the nearest station of 45 m. Average uncertainties in the north-south, east-west, and vertical directions were 134, 107, and 122 m.

Multiplets, November 4, 1600 PST, Through November 22, 1559 PST

As was the case for the previous time period, multiplets during this time period possessed lengthy lifespans that included long periods of quiescence (fig. 11). As before, many multiplets were concurrent. One of the most prominent multiplets during this period, F1, consisted of 3,269 events that began on November 4 at approximately 1700 PST and lasted for more than 20 days. The absolute location derived from first-arrival picks of earthquake stacks resulted in a location south of all other multiplets analyzed in this study. The emergent first arrivals in the earthquake stacks produced large pick uncertainties. Resulting large uncertainties in the absolute locations as a result of the large pick uncertainties means that we cannot distinguish the absolute hypocentroid of F1 from those of other multiplet locations. Relative relocations of F1 formed a tabular volume similar in shape to multiplet E7 (Oct. 16 start) (fig. 10*B*). The epicentral distribution of multiplet F1 had a long axis of approximately 100 m and a short axis of 20 m. The cluster was confined to depths of 260 to 300 m. Average uncertainties derived from jackknife analyses in the north-south, east-west, and vertical directions were 7.0, 15.1, and 10.2 m, respectively.

Discussion

Absolute Locations

The high-frequency nature of the earthquakes between September 23 and September 25, 2004, suggests that the earthquakes during this time period were fracturing brittle rock. Although the uncertainties in latitude and longitude are on the same order of magnitude as the epicentral shift between September 23 and September 25, we believe the phase pick differences outlined by Moran and others (this volume, chap. 2) support the observed shift in epicentroid location. The upward and southward migration of

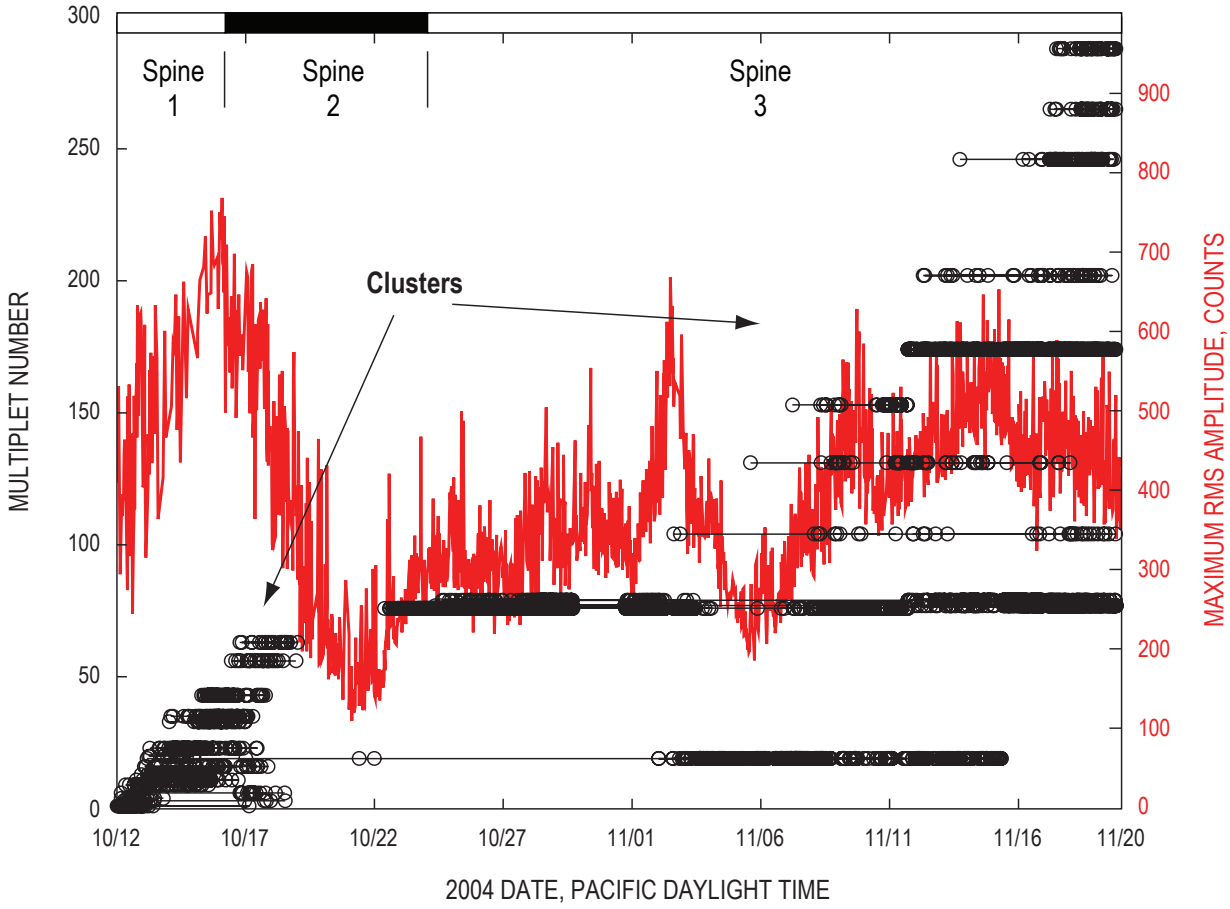

Figure 11. Timeline of multiplets detected on station ELK from October 12 through November 20, 2004. Each earthquake is plotted as a circle, and multiplets are identified by a horizontal line through events that define multiplet. Only multiplets that have more than 20 events are plotted. Maximum root-mean-squared (RMS) amplitude averaged over 1-minute intervals at station JUN shown in red. Date tickmarks are beginning of day, 0000 hr (midnight). Note change in amplitude scale compared to figures 4 and 8. Bar on top shows dome extrusion chronology (from Vallance and others, this volume, chap. 9).

absolute hypocenters between September 24 and September 26 and the shift to dominantly hybrid earthquakes suggest that the seismicity was occurring in response to a magmatic plug moving toward the surface (fig. 7). The shift occurred before any surface deformation near the 1980–86 dome (Dzurisin and others, this volume, chap. 14), although the continuous GPS at Johnston Ridge Observatory (JRO) did detect deflationary movement toward the volcano (Lisowski and others, this volume, chap. 15). An upward shift in hypocenters in the 1989 Ito-oki submarine eruption was explained as an upward propagating dike (Ukawa and Tsukahara, 1996). Their model showed that seismicity could occur above the crack tip in response to the dilatation of the crack below. Although this conclusion is plausible in hindsight at Mount St. Helens, the character and absolute locations of the earthquakes in the swarm between September 23 and September 25 alone probably would have not been enough to forecast an impending eruption.

After the first phreatic explosion on October 1, 2004, the loss of station SEP and consistently high seismic amplitudes on station YEL prevented the precise picking of events on crater stations. The absolute locations thus show greater scatter, have larger uncertainties, and are skewed in depth owing to the lessened station coverage. Jackknife tests performed by removing stations SEP and YEL from earthquake locations from September 25 to October 1 reveal depth patterns in seismicity similar to those seen for absolute earthquake locations calculated between October 1 and November 4. In essence, the precision in depth was poorer with the absence of stations SEP and YEL. This made relatively deep earthquakes deeper and shallow earthquakes become shallower (appendix 2). The locations were also more vertically aligned, similar to the absolute locations from October 1 through October 5 (fig. 3). The epicenter distribution in jackknife tests was nearly unchanged. We therefore suggest that the absolute locations for earthquakes from October 1 through October 5 were similar to those occurring before the first explosion. Similar tests indicate that locations for earthquakes after the October 5 explosion were similar to locations between September 25 and October 1 (appendix 2).

Absolute locations from November 5 to November 22 show that earthquake locations shifted slightly both up and south compared to pre-October 1 seismicity. The character of seismicity did not change significantly between October 16 and November 5, and we suggest that seismicity after the middle of October had similar absolute locations. The hypocentroid of absolute locations from November 5 to November 22 was ~290 m below the surface. Patterns in absolute locations between September 23 and November 22 indicate a conduit plunging 45º–60º northward at shallow depth beneath the old dome. The shape of the pattern is robust to changes in station layout (appendix 2); therefore we are confident the pattern is real.

Multiplets

A striking feature of seismicity during the early months of seismic unrest and eruption was the overwhelming presence of multiplets. Discrete multiplets occurred simultaneously throughout the study period; however, many can be further grouped into multiplet clusters. Here, we define a multiplet cluster as several multiplets that occurred simultaneously. Multiplet clusters often build slowly and end abruptly (figs. 4, 8, 11). On September 25, September 29, October 1, and October 5, the abrupt end of one cluster and the start of another was accompanied by changes in the amplitude of seismic signals recorded at station JUN (figs. 4, 8). No cluster recurred at any point during the study period, but in at least one case a multiplet within a previous cluster recurred after the cluster had ceased. The distinct clustering in time of multiplets may indicate that a particular source region was active during a cluster, with each multiplet having a different mechanism or occurring at a different location within the cluster source region. As each source region was altered or destroyed, a new cluster began from a new source region. Temporal clusters of multiplets were also observed at Soufrière Hills volcano, Montserrat, and were found to be related to the time derivative of the tilt (Green and Neuberg, 2006). Peaks in the real-time seismic amplitude measurement (RSAM), similar to the maximum amplitudes used here, were well correlated with peaks in the tilt at Soufrière Hills volcano; however, the relation between the RSAM and the occurrence of clusters of multiplets was not explicitly stated.

At Mount St. Helens, the absolute hypocentroid of each analyzed multiplet was similar when determined from stacks of each multiplet recorded at each station. All of the analyzed multiplets had locations within ~100 m of station BLIS at depths of 250 to 350 m (fig. 12). Further, the cross-correlation coefficients between each of the analyzed multiplets had values ranging between 0.17 and 0.50. This suggests that highly stable but distinct sources were present within a small source region at shallow depth beneath the 1980–86 dome. Similarly, the absolute location of multiplets that occurred at Soufrière Hills volcano in 1997 clustered tightly together, and Neuberg and others (2006) used this evidence to help argue for a pressure-dependent source for the occurrence of multiplets.

Multiplets also varied in lifespan. Generally, multiplets earlier in the study period had shorter lifespans than those occurring later. Lifespans of more than 1 month were observed for some multiplets during the dome-building phase of the eruption, suggesting a stable and stationary source region. Such long event families have only been reported at Shishaldin Volcano, Alaska (Petersen and others, 2006). However, very few studies have covered periods of time longer than days to weeks with continuous data. Amplitudes of events within individual multiplets were highly variable. However, changes typically varied smoothly with time. The magnitudes of events in large-population multiplets also ranged widely, from M_d –0.2 to M_d 3.0.

A steady decline in the cross-correlation coefficient between the first and subsequent events is observed in many multiplets. An example of this phenomenon is multiplet B1 (fig. 13). This change in cross-correlation coefficient could result from a shift in location or a change in the path between

an earthquake and the recording station. Gret and others (2005) exploited the sensitivity of the coda to changes in path to distinguish changes in location from changes in path at Mount Erebus, Antarctica. They compared the cross-correlation values of event families using windows in different parts of the earthquake waveform. A similar analysis of multiplets here reveals similar patterns in correlation coefficients of the first event to each subsequent event, regardless of the time window used (fig. 13). We therefore interpret the change in cross-correlation values with time to result from small changes in location that are within the uncertainty of our relative locations.

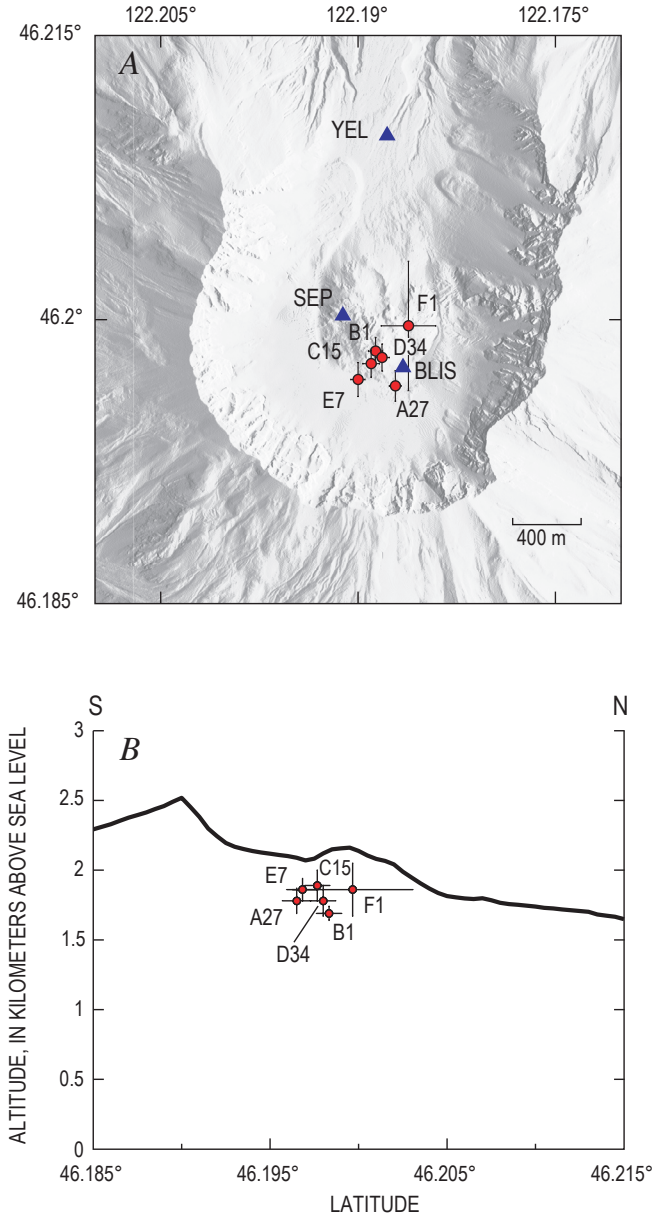

Figure 12. Absolute locations, obtained using first-arrival picks of event stacks, for multiplets depicted in figures 6 and 10. *A*, Map view. Blue triangles, permanent Pacific Northwest Seismic Network (PNSN) seismic stations as of November 4, 2004. *B*, Locations projected on north-south cross section through station SEP.

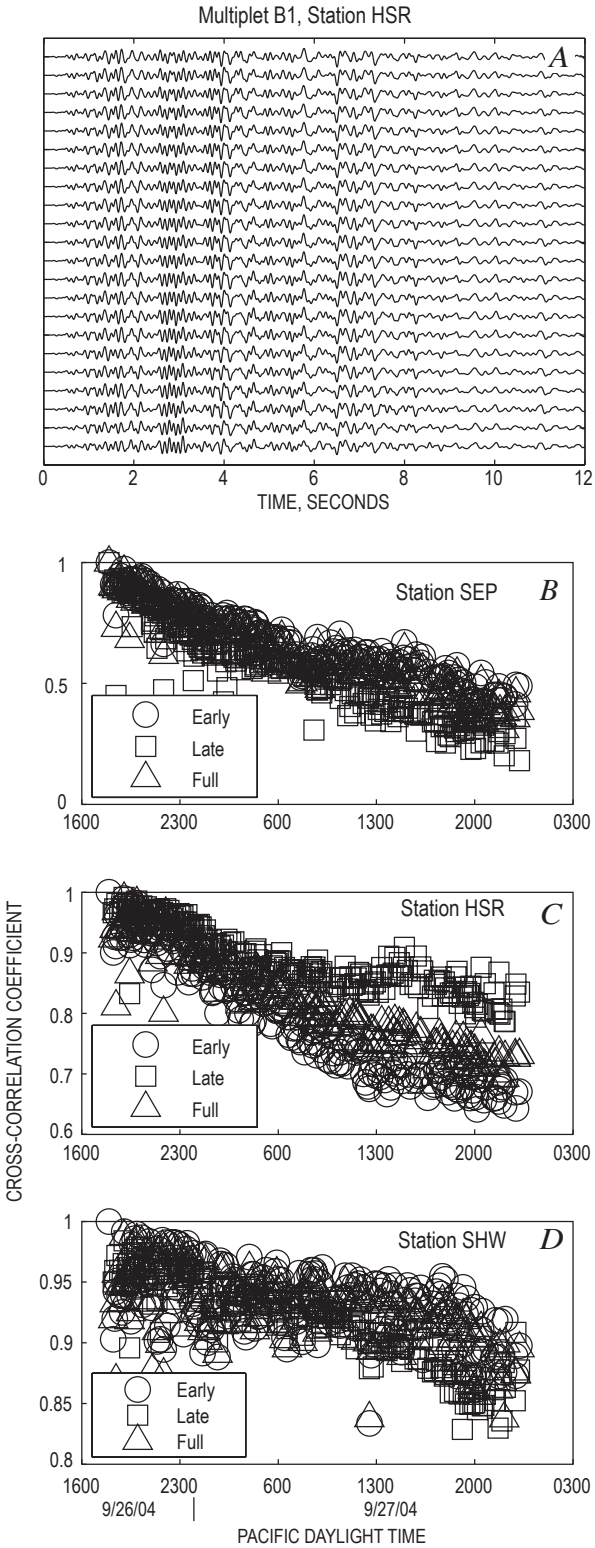

Figure 13. Cross-correlation analysis of first 220 events from multiplet B1. *A*, Waveforms filtered between 1 and 10 Hz of every tenth earthquake recorded on station HSR. *B–D*, Cross-correlation values as a function of time at stations SEP, HSR, and SHW, respectively. Three parts of waveform are used in each plot: first 4 s (early), next 4 s (late), and entire waveform (full).

Only the explosion on October 1 and, to a lesser extent, the explosion on October 5 significantly affected the occurrence of multiplets. After the October 1 explosion, all earthquakes, including multiplets, stopped for more than 3 hours (Moran and others, this volume, chap. 2). Several multiplets then restarted, and new multiplets began as the level of seismicity increased. This process repeated itself during periods of tremor and explosions occurring between October 1 and October 5; some multiplets already present continued and, in many cases, new multiplets began. The reactivation of multiplets and general seismicity after the October 1 explosion suggests that the phenomenon leading to the generation of multiplets during the time period around October 1 may be pressure dependent (Moran and others, this volume, chap. 2). The relation between the October 5 explosion and the occurrence of multiplets is less clear, because four multiplets continued through the explosion and another multiplet cluster started shortly after.

Relative locations of multiplets during the period we studied define a changing source volume. Between September 23 and October 5, hypocenters of multiplets defined a small equidimensional space, but after October 5 they defined larger, more tabular bodies striking west-southwest. In all cases except multiplet F1, depths spanned 20 m or less. The strike of the tabular bodies in E7 and F1 was also approximately perpendicular to the strike of spine 3, which extruded from October 24 to December 20, 2004 (Vallance and others, this volume, chap. 9). Such a progression is interesting in the context of volcanic activity. Moran and others (this volume, chap. 2) suggest that seismicity between September 23 and October 5 was associated with clearing of the conduit to allow subsequent lava extrusion. Smaller, more equidimensional source volumes early in the study period have relatively smaller surface area for gas escape. If the gas could not escape efficiently, excess overpressure may have caused fragmentation to occur in the conduit, resulting in the explosions seen between October 1 and October 5. After October 5, seismic amplitudes decreased, the lifespan of multiplets and source volumes increased, and extrusion of lava at the surface soon began. The tabular shape and orientation of the relative locations after October 1 are suggestive of a dike. Presumably, the larger source volume (and larger surface area) defined by the relative locations facilitated greater gas loss at shallow levels in the conduit, thereby contributing to steady degassing and suppression of explosions.

The cause for earthquakes at the restricted depths indicated by the absolute and relative locations is enigmatic. Seismogenic stresses around a plug of magma are dependent on the diameter, velocity, and viscosity of the plug (Webb and Dingwell, 1990; Goto, 1999). Indeed, it has been shown that stick-slip motion along the edges of an extruding plug can generate earthquakes that match the rates and sizes of observed drumbeat earthquakes at Mount St. Helens (Iverson, this volume, chap. 21). We might expect seismogenic zones at constrictions in the conduit (where the local magma flux increases), and we believe that this may be a reasonable source of seismogenic stress. We might also expect earthquakes in an area where the overburden pressure is low enough to allow solidification of the magma and force the viscosity across some threshold value. The viscosity is dependent mostly on pressure and, to a lesser extent, on temperature (Blundy and others, 2006). Viscosity can vary over many orders of magnitude, making it a difficult parameter to model in a context useful for interpreting the location of earthquakes (Goto, 1999). The lithostatic pressure, however, increased only slightly in the time period we describe. A decrease in the occurrence of earthquakes and multiplets after the October 1 explosion also suggests that the seismicity was dependent on pressure. We would therefore expect earthquake locations to remain fixed or to shallow slightly during the study period if the earthquakes were dependent on the lithostatic pressure, and the viscosity and velocity of the plug were fixed. The absolute depths of the multiplets were consistent with this observation and were also coincident with the depth of microlite crystallization of the rising magma (Cashman and others, this volume, chap. 19; Pallister and others, this volume, chap. 30). The depth of microlite crystallization is also thought to be a pressure-dependent phenomenon.

Not all earthquakes during the study period occurred as part of a multiplet. Indeed, the absolute locations show that earthquake hypocenters were spread across a wide range of depths, exceeding the depth range of the multiplets. The seismic energy declined after each explosion (Moran and others, this volume, chap. 6, their fig. 3), but for many of the explosions the multiplets persisted (fig. 8). This indicates that the earthquakes not associated with the multiplets declined in size and or number and therefore may also have been pressure dependent. Because the behavior of those earthquakes associated with multiplets and of those not associated with multiplets differs, we suggest that the cause of each phenomenon is distinct. In the case of the multiplets, the source is highly stable and nondestructive for long periods of time. In the case of earthquakes not associated with a multiplet, the source is nonrepeatable over short time scales.

Conclusions

Absolute and relative locations allowed us to characterize the possible source of earthquakes associated with renewed activity at Mount St. Helens beginning in September 2004. Absolute locations were improved with the use of a new velocity model. During periods of good depth constraint, absolute locations were found to be less than 1 km deep. A shallowing of earthquakes occurred between September 24 and 26, supported by changes in the difference of first-arrival picks at close-in stations (Moran and others, this volume, chap. 2). Absolute earthquake locations revealed a north-dipping structure which likely coincides with the shallow conduit that was formed during the initial vent-clearing phase.

Multiplets were prominent during the first months of the eruption. They included volcano-tectonic, hybrid, and low-

frequency events with a wide range of magnitudes. Multiplets varied in lifespan, but those of the vent-clearing phase had much shorter lifespans than multiplets occurring during dome extrusion. Multiplets also occurred in temporal clusters that were usually associated with large changes in the maximum RMS seismic-signal amplitude. Absolute locations derived from earthquake stacks show that the individual multiplets likely originated in nearly the same area. Relative locations showed source volumes with diameters on the order of 25 m before October 5 and larger, tabular source volumes oriented to the west-southwest thereafter, a change concurrent with the transition from vent clearing to dome building. In some cases, the cross-correlation coefficients of the first event compared to all subsequent events showed a steady decline, suggesting movement of the source location at a level within our uncertainty. The properties and locations of multiplets suggest that their occurrence was based on changes in pressure.

Acknowledgments

We wish to thank the staff at the Pacific Northwest Seismic Network for their meticulous work in collecting and archiving data and generating a consistent catalog throughout the volcanic sequence—notably Steve Malone, Tony Qamar, Amy Wright, Tom Yelin, Guy Medema, Karen Meagher, Bill Steele, Bob Norris, and Ruth Ludwin. We also wish to thank our reviewers, Seth Moran and Clifford Thurber, for insightful comments that significantly improved the final version of the manuscript, and Dave Ramsey for the map in figure 2.

References Cited

Aster, R.C., Borchers, B., and Thurber, C.H., 2005, Parameter estimation and inverse problems: Amsterdam, Elsevier Academic Press, 301 p.

Battaglia, J., Thurber, C.H., Got, J.-L., Rowe, C.A., and White, R.A., 2004, Precise relocation of earthquakes following the 15 June 1991 eruption of Mount Pinatubo (Philippines): Journal of Geophysical Research, v. 109, p. B07302, doi:10.1029/2003JB002959.

Blundy, J., Cashman, K., and Humphreys, M., 2006, Magma heating by decompression-driven crystallization beneath andesite volcanoes: Nature, v. 443, no. 7107, p. 76–80, doi:10.1038/nature05100.

Cashman, K.V., Thornber, C.R., and Pallister, J.S., 2008, From dome to dust; shallow crystallization and fragmentation of conduit magma during the 2004–2006 dome extrusion of Mount St. Helens, Washington, chap. 19 *of* Sherrod, D.R., Scott, W.E., and Stauffer, P.H., eds., A volcano rekindled; the renewed eruption of Mount St. Helens, 2004–2006: U.S. Geological Survey Professional Paper 1750 (this volume).

Dzurisin, D., Lisowski, M., Poland, M.P., Sherrod, D.R., and LaHusen, R.G., 2008, Constraints and conundrums resulting from ground-deformation measurements made during the 2004–2005 dome-building eruption of Mount St. Helens, Washington, chap. 14 *of* Sherrod, D.R., Scott, W.E., and Stauffer, P.H., eds., A volcano rekindled; the renewed eruption of Mount St. Helens, 2004–2006: U.S. Geological Survey Professional Paper 1750 (this volume).

Efron, B., and Gong G., 1983, A leisurely look at the bootstrap, the jackknife and cross-validation: American Statistician, v. 37, no. 1, p. 36–48.

Fréchet, J., 1985, Sismogenèse et doublets sismiques: Grenoble, France, Université Scientifique et Médicale de Grenoble, M.S. thesis, 206 p.

Frémont, M.J., and Malone, S.D., 1987, High precision relative locations of earthquakes at Mount St. Helens, Washington: Journal of Geophysical Research, v. 92, no. B10, p. 10223–10236.

Geller, R.J., and Mueller, C.S., 1980, Four similar earthquakes in central California: Geophysical Research Letters, v. 7, p. 821–824.

Got, J.-L., Fréchet J., and Klein, F.W., 1994, Deep fault plane geometry inferred from multiplet relative relocation beneath the south flank of Kilauea: Journal of Geophysical Research, v. 99, no. B8, p. 15375–15386.

Goto, A., 1999, A new model for volcanic earthquake at Unzen volcano; melt rupture model: Geophysical Research Letters, v. 26, no. 16, p. 2541–2544.

Green, D.N., and Neuberg, J., 2006, Waveform classification of volcanic low-frequency earthquake swarms and its implication at Soufrière Hills Volcano, Montserrat: Journal of Volcanology and Geothermal Research, v. 153, nos. 1–2, p. 51–63, doi: 10.1016/j.jvolgeores.2005.08.003.

Gret, A., Snieder, R., Aster, R.C., and Kyle, P.R., 2005, Monitoring rapid temporal change in a volcano with coda wave interferometry: Geophysical Research Letters, v. 32, L06304, doi: 10.1029/2004GL0211143.

Herrmann, R.B., 1979, FASTHYPO—a hypocenter location program: Earthquake Notes, v. 50, no. 2, p. 25–37.

Iverson, R.M., 2008, Dynamics of seismogenic volcanic extrusion resisted by a solid surface plug, Mount St. Helens, 2004–2005, chap. 21 *of* Sherrod, D.R., Scott, W.E., and Stauffer, P.H., eds., A volcano rekindled; the renewed eruption of Mount St. Helens, 2004–2006: U.S. Geological Survey Professional Paper 1750 (this volume).

Klein, F.W., 1989, HYPOINVERSE, a program for VAX computers to solve for earthquake locations and magnitudes: U.S. Geological Survey Open-File Report 89–314, 59 p.

Lahr, J.C., Chouet, B.A., Stephens, C.D., Power, J.A., and Page, R.A., 1994, Earthquake classification, location, and error analysis in a volcanic environment; implications for the magmatic system of the 1989–1990 eruptions at Redoubt Volcano, Alaska: Journal of Volcanology and Geothermal Research, v. 62, nos. 1–4, p. 137–151, doi:10.1016/0377-0273(94)90031-0.

Lees, J.M., and Crosson, R.S., 1989, Tomographic inversion for three-dimensional velocity structure at Mount St. Helens using earthquake data: Journal of Geophysical Research, v. 94, no. B5, p. 5716–5728.

Lisowski, M., Dzurisin, D., Denlinger, R.P., and Iwatsubo, E.Y., 2008, Analysis of GPS-measured deformation associated with the 2004–2006 dome-building eruption of Mount St. Helens, Washington, chap. 15 *of* Sherrod, D.R., Scott, W.E., and Stauffer, P.H., eds., A volcano rekindled; the renewed eruption of Mount St. Helens, 2004–2006: U.S. Geological Survey Professional Paper 1750 (this volume).

Malone, S.D., and Pavlis, G.L., 1983, Velocity structure and relocation of earthquakes at Mount St. Helens [abs.]: Eos (American Geophysical Union Transactions), v. 64, p. 895.

McChesney, P.J., Couchman, M.R., Moran, S.C., Lockhart, A.B., Swinford, K.J., and LaHusen, R.G., 2008, Seismic-monitoring changes and the remote deployment of seismic stations (seismic spider) at Mount St. Helens, 2004–2005, chap. 7 *of* Sherrod, D.R., Scott, W.E., and Stauffer, P.H., eds., A volcano rekindled; the renewed eruption of Mount St. Helens, 2004–2006: U.S. Geological Survey Professional Paper 1750 (this volume).

Michelini, A., and Lomax, A., 2004, The effect of velocity structure errors on double-difference earthquake location: Geophysical Research Letters, v. 31, L09602, doi:10.1029/2004GL019682.

Moran, S.C., Malone, S.D., Qamar, A.I., Thelen, W.A., Wright, A.K., and Caplan-Auerbach, J., 2008a, Seismicity associated with renewed dome building at Mount St. Helens, 2004–2005, chap. 2 *of* Sherrod, D.R., Scott, W.E., and Stauffer, P.H., eds., A volcano rekindled; the renewed eruption of Mount St. Helens, 2004–2006: U.S. Geological Survey Professional Paper 1750 (this volume).

Moran, S.C., McChesney, P.J., and Lockhart, A.B., 2008b, Seismicity and infrasound associated with explosions at Mount St. Helens, 2004–2005, chap. 6 *of* Sherrod, D.R., Scott, W.E., and Stauffer, P.H., eds., A volcano rekindled; the renewed eruption of Mount St. Helens, 2004–2006: U.S. Geological Survey Professional Paper 1750 (this volume).

Musumeci, C., Gresta, S., and Malone, S.D., 2002, Magma system recharge of Mount St. Helens from precise relative hypocenter location of microearthquakes: Journal of Geophysical Research, v. 107, no. B10, 2264, p. ESE 16-1–16-9, doi:10.1029/2001JB000629.

Neuberg, J.W., Tuffen, H., Collier, L., Green, D., Powell, T., and Dingwell, D., 2006, The trigger mechanism of low-frequency earthquakes on Montserrat: Journal of Volcanology and Geothermal Research, v. 153, nos. 1–2, p. 37–50, doi:10.1016/j.jvolgeores.2005.08.008.

Pallister, J.S., Thornber, C.R., Cashman, K.V., Clynne, M.A., Lowers, H.A., Mandeville, C.W., Brownfield, I.K., and Meeker, G.P., 2008, Petrology of the 2004–2006 Mount St. Helens lava dome—implications for magmatic plumbing and eruption triggering, chap. 30 *of* Sherrod, D.R., Scott, W.E., and Stauffer, P.H., eds., A volcano rekindled; the renewed eruption of Mount St. Helens, 2004–2006: U.S. Geological Survey Professional Paper 1750 (this volume).

Pearson, C.F., and Kienle, J., 1978, A seismic refraction study of Augustine volcano, Alaska [abs.]: Eos (American Geophysical Union Transactions), v. 59, no. 4, p. 311.

Petersen, T., Caplan-Auerbach, J., and McNutt, S.R., 2006, Sustained long-period seismicity at Shishaldin Volcano, Alaska: Journal of Volcanology and Geothermal Research, v. 151, p. 365–381.

Poupinet, G., Ellsworth, W.L., and Fréchet, J., 1984, Monitoring velocity variations in the crust using earthquake doublets; an application to the Calaveras Fault, California: Journal of Geophysical Research, v. 89, p. 5719–5731.

Pujol, J., 2000, Joint event location–the JHD technique and applications to data from local seismic networks, *in* Thurber, C.H., and Rabinowitz, N., eds., Advances in seismic event location: Dordrecht, Kluwer Academic Publishers, p. 163–204.

Qamar, A.I., Malone, S.D., Moran, S.C., Steele, W.P., and Thelen, W.A., 2008, Near-real-time information products for Mount St. Helens—tracking the ongoing eruption, chap. 3 *of* Sherrod, D.R., Scott, W.E., and Stauffer, P.H., eds., A volcano rekindled; the renewed eruption of Mount St. Helens, 2004–2006: U.S. Geological Survey Professional Paper 1750 (this volume).

Reeder, J.W., and Lahr, J.C., 1987, Seismological aspects of the 1976 eruption of Augustine Volcano, Alaska: U.S. Geological Survey Bulletin 1768, 32 p.

Rowe, C.A., Thurber, C.H., and White, R.A., 2004, Dome growth behavior at Soufriere Hills Volcano, Montserrat, revealed by relocation of volcanic event swarms, 1995–1996: Journal of Volcanology and Geothermal Research, v. 134, no. 3, p. 199–221.

Schaff, D.P., Bokelmann, G.H.R., Ellsworth, W.L., Zanzerkia, E., Waldhauser, F., and Beroza, G.C., 2004, Optimizing correlation techniques for improved earthquake location: Bulletin of the Seismological Society of America, v. 94, no. 2, p. 705–721.

Stephens, C.D., and Chouet, B.A., 2001, Evolution of the December 14, 1989 precursory long-period event swarm at Redoubt Volcano, Alaska: Journal of Volcanology and Geothermal Research, v. 109, p. 133–148.

Swanson, D.A., Casadevall, T.J., Dzurisin, D., Malone, S.D., Newhall, C.G., and Weaver, C.S., 1983, Predicting eruptions at Mount St. Helens, June 1980 through December 1982: Science, v. 221, no. 4618, p. 1369–1376.

Thelen, W.A., Malone, S.D., Qamar, A.I., and Pullammanappallil, S., 2006, Improvements to absolute locations from an updated velocity model at Mount St. Helens, Washington [abs.]: Seismological Research Letters, v. 77, no. 2, p. 238.

Ukawa, M., and Tsukahara, H., 1996, Earthquake swarms and dike intrusions off the east coast of Izu Peninsula, central Japan: Tectonophysics, v. 253, p. 285–303.

Vallance, J.W., Schneider, D.J., and Schilling, S.P., 2008, Growth of the 2004–2006 lava-dome complex at Mount St. Helens, Washington, chap. 9 *of* Sherrod, D.R., Scott, W.E., and Stauffer, P.H., eds., A volcano rekindled; the renewed eruption of Mount St. Helens, 2004–2006: U.S. Geological Survey Professional Paper 1750 (this volume).

Waite, G.P., and Moran, S.C., 2006, Crustal P-wave speed structure under Mount St. Helens from local earthquake tomography [abs.]: Eos (American Geophysical Union Transactions), v. 87, no. 52, Fall Meeting supplement, Abstract V11B-0578.

Waldhauser, F., 2001, HypoDD—a program to compute double-difference hypocenter locations (hypoDD version 1.0): United States Geologic Survey Open-File Report 01–113, 25 p.

Waldhauser, F., and Ellsworth, W.L., 2000, A double-difference earthquake location algorithm; method and application to the northern Hayward Fault, California: Bulletin of the Seismological Society of America, v. 90, p. 1353–1368.

Webb, S.L., and Dingwell, D.B., 1990, Non-Newtonian rheology of igneous melts at high stress and strain rates; experimental results for rhyolite, andesite, basalt, and nephelinite: Journal of Geophysical Research, v. 95, p. 15695–15701.

Williams, D.L., Abrams, G., Finn, C., Dzurisin, D., Johnson, D.J., and Denlinger, R., 1987, Evidence from gravity data for an intrusive complex beneath Mount St. Helens: Journal of Geophysical Research, v. 92, no. B10, p. 10207–10222.

Wolfe, C.J., 2002, On the mathematics of using difference operators to relocate earthquakes: Bulletin of the Seismological Society of America, v. 92, p. 2879–2892.

Appendix 1. Velocity Model

A velocity model serves an integral role in earthquake locations. Although many regions have three-dimensional velocity models available, computing power and speed requirements often mean that one-dimensional velocity models are used for routine locations. At Mount St. Helens, large static station corrections and earthquakes with locations above the velocity model datum (airquakes) were common during the beginning of the 2004 unrest and eruption, which demonstrated the need for a more accurate velocity model in the shallow part of the volcano. The velocity model used for routine locations by the Pacific Northwest Seismic Network (PNSN) was determined using nearby quarry blasts (Malone and Pavlis, 1983). That velocity model is regionally accurate, judging from the small station corrections on stations beyond the edifice of Mount St. Helens. The data used for the velocity model, however, had poor ray coverage through the shallow part of the edifice (<2 km). The result is a constant P-wave velocity of 4.6 km/s in the upper 2.2 km of the velocity model, far too fast for the pyroclastic deposits, thin lava flows, and fractured dacite lava domes found throughout the crater walls of the volcano. Exceedingly fast velocities resulted in large station corrections on edifice and crater stations used for routine processing (table 2). Three-dimensional P-wave velocity models exist for Mount St. Helens (Lees, 1989; Waite and Moran, 2006), but they also suffer from a lack of ray coverage and coarse resolution at the depths we are studying. Here we describe the method we used to develop a shallow (<2 km) one-dimensional P-wave velocity model to supplement the existing one-dimensional model (in use by the PNSN) for the Mount St. Helens area.

Table 2. Station corrections calculated for each velocity model with permanent Pacific Northwest Seismic Network (PNSN) stations used in routine earthquake locations between 2004 and 2006.

[See McChesney and others (this volume, chap. 7) for locations of seismic stations not shown in figure 2. Data shown here for each station are time residuals, in seconds, that result from the inadequacy of a one-dimensional model to represent the three-dimensional Earth. In theory, station residuals converge to zero as the computed velocity model converges toward the actual velocity structure between earthquake and station.]

PNSN Station	Existing PNSN Model[1] (s)	New Velocity Model[1] (s)	New Velocity Model[2] (s)
SEND	-0.087	0.000	-0.023
RAFT	-0.187	-0.083	0.063
MIBL	-0.218	-0.096	0.000
WESG	-0.179	-0.091	0.099
MIDE	-0.212	-0.190	0.000
SEP	-0.151	-0.102	0.071
BLIS	-0.393	-0.366	-0.170
NED	-0.050	0.000	0.131
SUG	0.200	0.000	0.064
YEL	0.024	0.000	0.078
EDM	0.179	0.059	0.033
HSR	0.192	0.070	0.088
SHW	0.108	0.042	-0.032
STD	0.070	0.057	0.000
SOS	0.017	0.039	0.000
JUN	-0.029	0.025	-0.034
FL2	-0.029	0.054	0.000
CDF	-0.043	0.134	0.062
ELK	-0.226	-0.177	-0.227
TDL	-0.163	-0.158	-0.223
LVP	-0.078	0.000	-0.060

[1]Datum is 1,700 m above sea level.

[2]Datum is 2,200 m above sea level.

Methods

In the summer of 2005, we deployed, at 100-m intervals, 39 RT-125 seismic recorders with alternating 4.5-Hz geophones and 1-Hz vertical seismometers (Thelen and others, 2006). The instruments were deployed for three days. The array began approximately 1 km north of the 2004–5 vent and extended northward 4 km onto the Pumice Plain (fig. 14).

We used an Occam's inversion scheme with second-order Tikhonov regularization to invert first-arrival data for a velocity model (Aster and others, 2005). The Occam's inversion scheme seeks a solution to $G(m) = d$ subject to the following constraints:

$$min \left\| Lm \right\|_2$$

$$\text{and} \left\| G(m) - d \right\|_2 \leq \delta ,$$

where $G(m)$ is a function of the model parameters that calculates the data, d, from the model. In this formulation, L is the roughening matrix (which is equal to the finite-difference approximation of the second derivative), and δ is the discrepancy parameter, $\sigma\sqrt{n}$, where n is the number of degrees of freedom and σ is the uncertainty of the time picks. Occam's inversion relies on an iteratively applied local linearization given by Taylor's theorem,

$$G(m^k + \Delta m) \approx G(m^k) + J(m^k)\Delta m \ ,$$

where m^k is a trial model and $J(m^k)$ is the Jacobian. Using a damped least-squares approach, the constraints above, combined with the Taylor approximation, give

$$\min \left\| G(m^k) + J(m^k)\Delta m - d \right\|_2^2 + \alpha^2 \left\| L(m^k + \Delta m) \right\|_2^2 \ ,$$

where the parameter α is adjusted after each iteration so that the solution will not exceed the allowable misfit. The inversion is terminated when $\delta^2 = \chi^2$, where

$$\chi^2 = \sum_{i=1}^{m} \frac{(d_i - (Gm_{L_2})_i)^2}{\sigma_i^2} .$$

Our "active sources" were earthquakes associated with dome building at Mount St. Helens. Twenty $M_d > 1.0$ earthquakes occurred within the crater from the surface to depths of 1 km while our instruments were recording. Of these, we chose the best earthquake (August 20, 2005, 21:28:37 PDT; $M_d = 2.6$) on the basis of its clarity of impulsive arrivals across the transect and the number of PNSN catalog picks used to routinely locate the earthquake. The epicenter of the earthquake is well constrained, owing to the excellent azimuthal coverage of seismometers around Mount St. Helens. The existing one-dimensional velocity model described above, however, allows for a tradeoff between the depth and the origin time within the upper 2.2 km of the velocity model. Thus, the depth is not as well constrained as the epicenter. With additional layers in the shallow part of the velocity model, this tradeoff is less important.

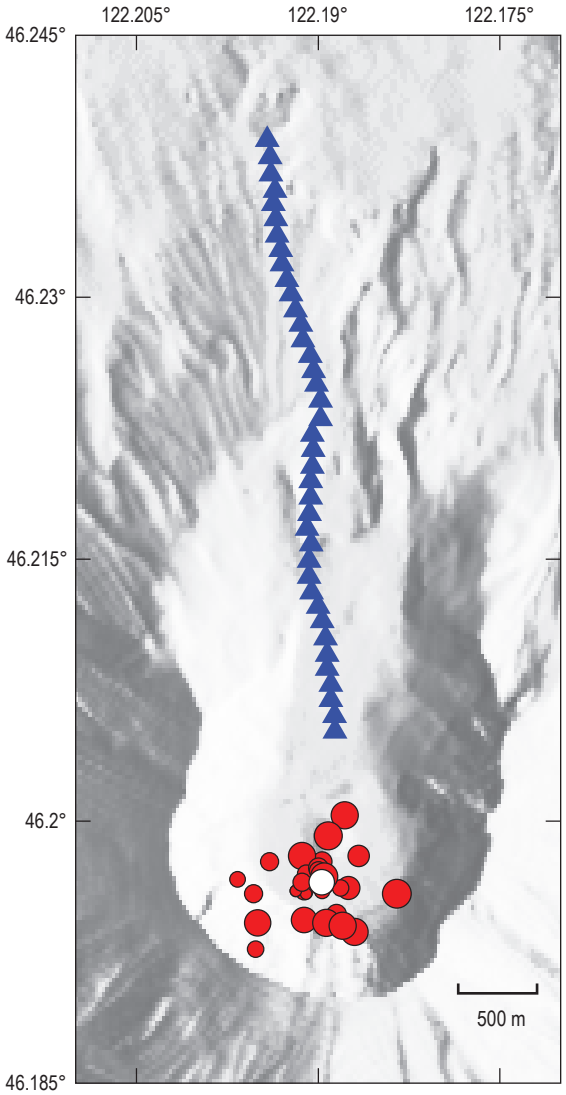

Figure 14. Instrument layout (blue triangles) with earthquake epicenters (red dots) used for P-wave inversion. Epicenter of primary earthquake used in inversion is shown by white dot.

Secondary arrivals were observed in the record section of the transect, but they were not easily picked across the array. We therefore used only the P-wave arrivals. Errors in picking first arrivals on the event used for the inversion were assumed to be constant and were estimated to be within five time samples (0.05 s) of the actual arrival. Our algorithm allows for the use of one earthquake at a time. We chose to use only one earthquake in our inversion for two reasons: (1) there was only one other earthquake (August 22, 2005, 03:32:45 PDT; $M_d = 1.4$) that possessed impulsive arrivals across the entire transect, and (2) that earthquake showed an identical pattern in first-arrival picks to the earthquake we used for the inversion. Using multiple earthquakes would not change or add to the information used in the inversion because the earthquakes that occurred during the deployment of the transect occurred in such a tight cluster. First arrivals from the other earthquakes that occurred during the deployment were picked only if they could be identified with a precision of better than 0.05 s. The time spread in picks at a given offset was used to define the standard deviation to ensure that the inversion did not overfit the data.

We used a one-dimensional travel-time calculator parameterized with constant velocity layers. The travel-time calculator allows for a three-dimensional geometry of stations and earthquake location. The setup of the inverse problem prescribes node depths and solves for the layer velocity between nodes. The node number and depths were based largely on constraints imparted by the program used for earthquake locations, SPONG. The first constraint is the use of a total of 10 layers in the velocity model. When combined with the existing PNSN velocity model, this only allowed for 4 layers. The second constraint is that different station altitudes can be used, but they must be included inside the top layer of the velocity model. Stations within 10 km of the crater, excluding the crater stations, span altitudes from 1,268 m to 1,700 m. We thus required a 500-m-thick top layer so that we could include the altitudes of these closest stations to the crater. Depths of the remaining three node-depths layers were found through a grid search with an increment of 100 m. The preferred model is the model that satisfies the condition above and has the smallest residual times ($t_{observed} - t_{calculated}$). Models with low-velocity inversions were poorly constrained using first-arrival data and thus were not considered.

The initial depth of the earthquake used in the inversion was 0.24 km (datum at 1,700 m above sea level). We iterated velocity-model solutions, each time updating the station corrections using a subset of PNSN catalog earthquakes with high-quality arrivals (see station correction discussion below) to get a new earthquake location and origin time. The new earthquake parameters were then used to update distance and time information of the transect, and the

velocity model inversion was run again. Iterations stopped when the change in depth between iterations was less than the calculated uncertainty of the solution. The final depth of the earthquake was calculated to be 0.13 km. By alternately recalculating the location and the velocity model, we minimize errors in the location of the earthquake and in the velocity inversion results.

Location uncertainties in our nonlinear velocity inversion were calculated using the diagonal of the covariance, a method that is appropriate in linear inverse problems. We adapted this technique to our problem by linearizing the solution through a central difference and then calculating the error as if it were a linear problem. This approach is often used, though not strictly correct, and may underestimate the uncertainties in the model (Aster and others, 2005).

Station corrections are static time corrections used in earthquake hypocenter inversions using one-dimensional velocity models. Station corrections, which compensate for the one-dimensional modeling of a truly three-dimensional velocity structure, can be minimized by finding the closest one-dimensional approximation of the three-dimensional velocity structure under the volcano (Pujol, 2000). We do not minimize the station corrections here; however, we do use decreases in station corrections as a proxy for the quality of our velocity model.

Station corrections were calculated using a subset of 29 PNSN catalog events that occurred between 2004 and 2006. These events were selected for their exceptionally sharp impulsive arrivals and were already in use for calibrating PNSN velocity models for Mount St. Helens (S. Malone, oral commun., 2006). The first arrivals of these events were picked on the PNSN stations only if the arrival was unambiguous to ±0.05 s. Locations were then calculated using the existing velocity model and station corrections. The new velocity model was then used with the existing, fixed location to calculate new residuals for each station for each event. The station residuals were then averaged across events to obtain the station correction. This approach is not without flaws. Earthquake locations using the old velocity model may have errors imparted by the velocity model itself, which would lead to a bias in the station corrections. Near-site effects may also introduce a bias in the station corrections. Despite these disadvantages, we find that comparing station corrections gives us the best measure of spatial quality between two velocity models.

Results

P-Wave Model

The final result of our P-wave velocity inversion is shown in figure 15. Disappointingly, our inversion did not constrain velocities deeper than 1.5-km depth. This is because of the lack of deep earthquakes during the deployment and the final length of the transect used. Our deepest velocity (5.12 km/s) agrees well with the shallowest velocity of the existing model that spans depths of 0 to 2.2 km. Inverting a subset of the 12 closest picks to the hypocenter resulted in shallow velocities as low as 2.4 km/s, instead of the 2.7 km/s that is calculated in the final model. Residuals of the model show trends imparted by the constant velocity layers used in the inversion. The 13 picks farthest from the hypocenter show apparent velocities that are abnormally high (7–8 km/s). In our inversion, we discarded points (seven in all) with the largest offsets until inverted velocities at depths of 1 to 1.5 km below the transect were reasonable with respect to the existing velocity model. Removing time picks from the most distant stations resulted in depth constraints that were not as deep as we had initially planned, but it was required in order to get reasonable results. The apparent high velocities in our time picks may be a result of three-dimensional variations in wave speed. An alternative explanation may be a large amount of scattering that is shifting the energy of the direct arrival later in the signal and masking the energy remaining in the actual first arrival buried in the noise. Three-dimensional effects are also seen near the 2.1-km offset (fig. 15*A*), where three picks are advanced with respect to surrounding picks.

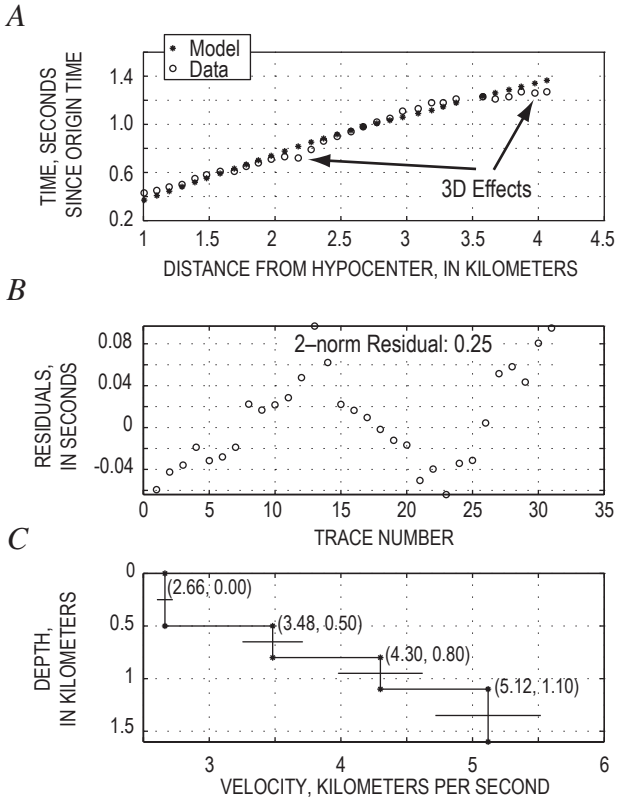

Figure 15. Results of final velocity inversion and grid search for P-wave model. *A*, Comparison of data (circles) and model (stars) for the final model. *B*, Plot of residuals. *C*, Velocity model plotted with 90-percent confidence intervals shown as horizontal lines.

Discussion

The results of our P-wave model show velocities of 2.4–2.7 km/s in the uppermost layer, approximately 1 km/s slower than found in the velocity model used at Mount St. Helens by Musumeci and others (2002). The discrepancy is due to different ray coverage within the crater. In our inversion, we had 39 instruments draping the crater floor and flank and recorded earthquakes less than 1 km deep. In the velocity model by Musumeci and others (2002), only three stations existed inside the crater and only earthquakes deeper than 2.5 km were recorded. The P waves used in our study thus better sampled the shallow structure of the volcano. Our shallowest velocities are similar to those measured at other volcanoes, including Augustine Volcano, Alaska (2.24–2.6 km/s; Pearson and Kienle, 1978), Redoubt Volcano, Alaska (2.9 km/s; Lahr and others, 1994), and Soufrière Hills, Montserrat (2.17 km/s; Rowe and others, 2004).

The new P-wave velocity model has relatively high velocities (4.3 km/s) at fairly shallow depths (0.8 km), considering the volcanic strata exposed within the crater. But such high velocities may be warranted, inasmuch as an intrusive suite at approximately 1-km depth has been interpreted from gravity data (Williams and others, 1987). Velocities of approximately 5.1 km/s have also been used in layered velocity models at Augustine Volcano at 0.9-km depth (Reeder and Lahr, 1987) and at Redoubt Volcano at 0.6-km depth (Lahr and others, 1994). Furthermore, the new P-wave model shows decreases in calculated station corrections at all stations on the volcano, suggesting that the new model is a closer approximation of the three-dimensional velocity structure under the edifice than the existing PNSN model (table 2).

By concatenating the existing S4 velocity model from the PNSN onto the bottom of the inverted velocity model, we are able to calculate improvements to station corrections resulting from the new model (table 2). The altitudes of our transect ranged between 1,100 m and 1,800 m above sea level. At best, our data only constrain the seismic velocities up to the maximum altitude of our transect. For consistency with the existing PNSN velocity model, we set our initial datum to 1,700 m. To allow for earthquake locations inside the new dome, we also considered a model identical to the final inverted velocity model, except with a datum at 2,200 m (datum-adjusted). The layer above the initial datum (1,700 m) has a constant velocity equal to the uppermost layer (2.66 km/s), and the layer depths are adjusted according to the new datum. Adjusting the datum to 2,200 m above sea level, the altitude of the highest seismic station, led to reduced station corrections. In particular, the station corrections on the dome are greatly reduced with respect to other velocity models we considered (table 2). The datum-adjusted model is preferred because it allows for earthquake locations within the new dome and results in lower station corrections for stations on the edifice and inside the crater. Admittedly, no dome material was present at 2,200-m altitude early in the study period, but in order to present the most consistent set of locations for the entire study period, a consistent velocity model should be used throughout the study period.

Appendix 2. Effect of Changing Station Configurations

We simulated the results of changing station configurations within the crater using PNSN catalog events from November 4 through November 20, 2004. During this time period, stations BLIS, YEL, and SEP were operational (McChesney and others, this volume, chap. 7), allowing an opportunity to understand the effect of particular stations on the geometry of the absolute locations. Absolute locations from September 23 until October 1 all lie along a north-dipping structure that descends beneath the 1980–86 dome. When good station coverage and impulsive arrivals were both present starting around November 4, 2004, a similar north-dipping structure emerged (fig. 16*A*). This north-dipping structure was found to be fairly robust analytically, persisting even when the two closest stations were excluded (figs. 16*B*, *C*). Only when station YEL is also excluded is there a breakdown in the shape of the cluster.

Generally, as we removed the close stations, the hypocentroid of the cluster moved deeper and the range of depths grew larger. For example, the original locations had a hypocentroidal depth of ~290 m. Upon removing station BLIS from calculation, the hypocentroid deepened to ~350 m. When both SEP and BLIS were removed, the hypocentroid was more than 400 m deep.

Appendix 3. Jackknife Tests

We show here the results of jackknife tests on the multiplet E7. The original relative locations show a tabular body with a surface projection spanning nearly 50 m. In depth the locations are restricted to a range of only about 20 m, outlining a cigar-shaped source region (figs. 10*B*, 17*A*). Multiplets D34 and F1 also show similar tabular bodies, so we are compelled to show the results of our jackknife tests to prove that the locations are not an artifact of station geometry or poor waveform alignment. In figure 17, we show the results of removing, one at a time, each of the four stations with the most observations. In almost all cases there is no change in the geometry of the source region. An exception is the source geometry when station YEL is removed (fig. 17*C*). In this test, the orientation of the source region is more southwest than in the original locations, and the relative hypocenters, viewed to the east, are elongate north-south.

We also tested the effect of a P-wave velocity model on the relative locations (fig. 17*F*). As mentioned previously, the velocity model that we chose lacks layer boundaries near the cluster centroid, so a change to higher velocities simply spreads the hypocenters out over a larger area without gross change in geometry.

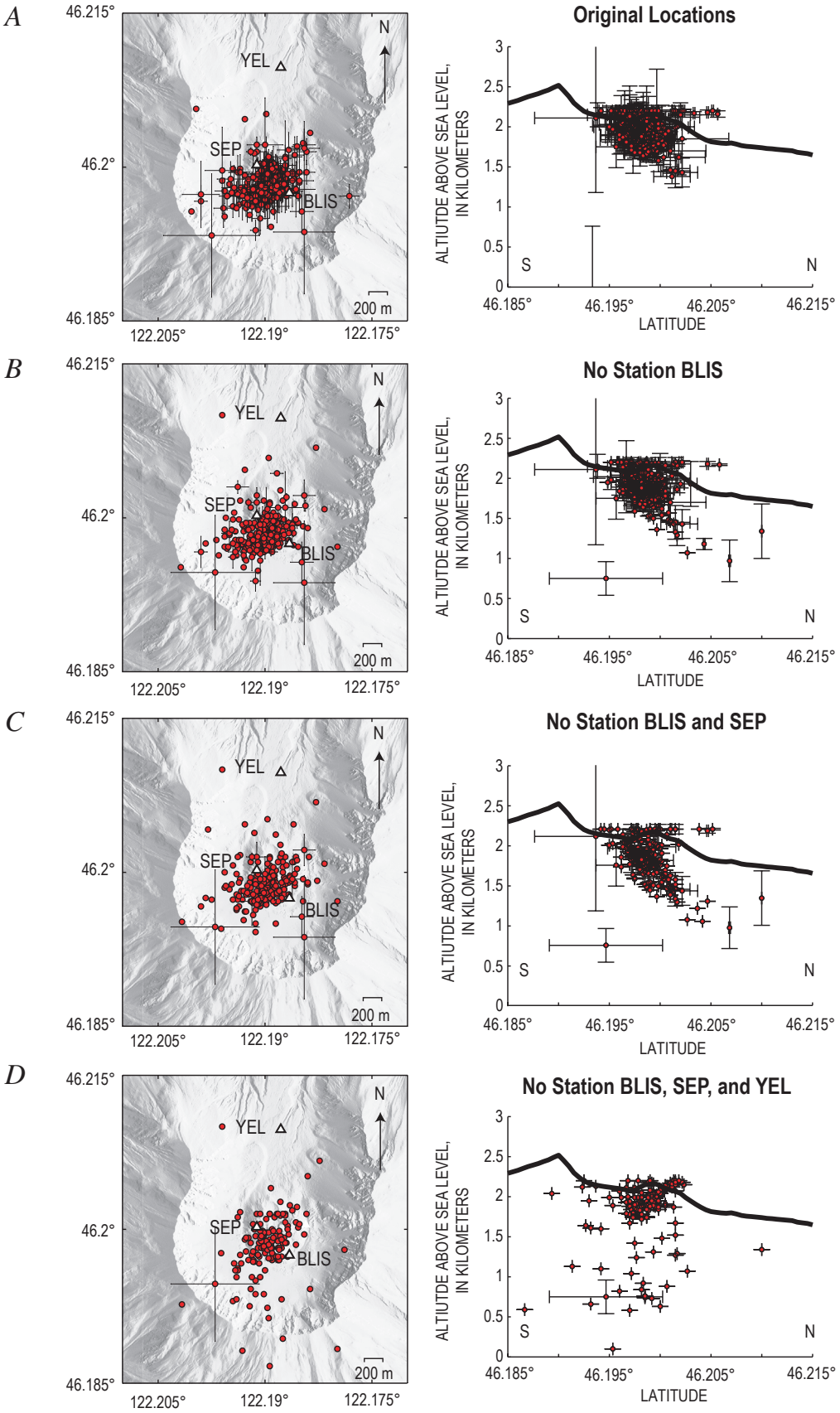

Figure 16. (*A–D*) Results of simulations of different station configurations using Pacific Northwest Seismic Network (PNSN) catalog earthquakes from November 4, 2004, to November 20, 2004.

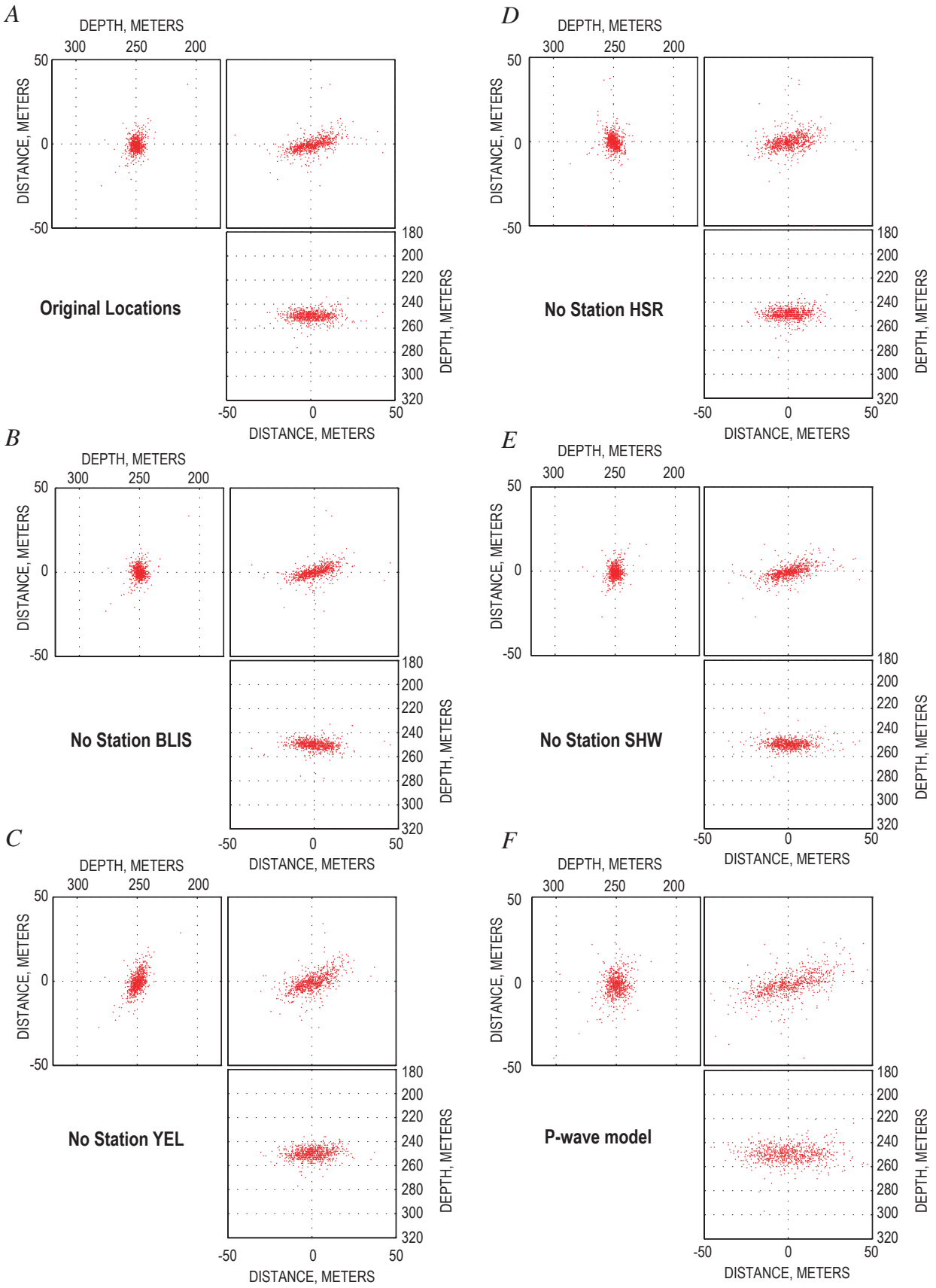

Figure 17. (*A–E*) Results of jackknife tests on multiplet E7. *F,* Results of the use of a P-wave model in the relative locations of multiplet E7.